#### RESEARCH



# Collapse and slow recovery of the Atlantic Meridional Overturning Circulation (AMOC) under abrupt greenhouse gas forcing

Paul Edwin Curtis<sup>1</sup> • Alexey V. Fedorov<sup>1,2</sup>

Received: 8 February 2023 / Accepted: 4 March 2024 © The Author(s), under exclusive licence to Springer-Verlag GmbH Germany, part of Springer Nature 2024

#### Abstract

Modeling studies which abruptly increase atmospheric CO<sub>2</sub> concentration evidence a rapid reduction or collapse of the Atlantic Meridional Overturning Circulation (AMOC) from its present state of strong overturning circulation into one characterized by a nearly absent deep ocean overturning in the Atlantic and a reduced northward heat transport. Similar transitions are frequently discussed in the context of both present and past global climate changes. Far less discussed, however, is the eventual recovery of the circulation and the establishment of a new equilibrium state, which may occur, or not, many millennia following the initial collapse. Here, we use the Community Earth System Model (CESM1) and a range of abrupt CO<sub>2</sub> forcing scenarios (0.5xCO<sub>2</sub>, and 2xCO<sub>2</sub> up to 16xCO<sub>2</sub>) to evaluate the timescales, and the factors influencing these timescales, in the AMOC's slow evolution to equilibrium. This takes ~ 2000 years for 2xCO<sub>2</sub>, but over 10,000 years for 8xCO<sub>2</sub> in the model. We focus on the interplay between upper- and deep-ocean temperature and salinity, and Arctic sea ice, to diagnose the mechanisms of AMOC recovery and its transition towards equilibrium. We show that the freshening of the Arctic and Subpolar region can delay or possibly halt AMOC recovery. Critically, even after radiative balance is reached at the top of the atmosphere, ocean temperature and salinity keep evolving for thousands of years, affecting the AMOC. These results highlight the long timescales needed for ocean adjustment to radiative forcing, and also shed light on AMOC characteristics in past climates with atmospheric CO<sub>2</sub> concentrations markedly different from the present day.

**Keywords** Atlantic Meridional Overturning Circulation · Equilibrium climate change · Ocean dynamics · General circulation models · Climate change

#### 1 Introduction

A key component of the global climate system, the Atlantic Meridional Overturning Circulation (AMOC) is the critical branch of the deep ocean circulation in the Atlantic (Rahmstorf 2002; Buckley and Marshall 2016). The AMOC transports heat throughout the Atlantic basin (Trenberth et al. 2019), and influences a broad range of weather and climate phenomena, including the atmospheric jet stream (Liu et al. 2020), and Atlantic hurricanes (Yan et al. 2017), the Intertropical Convergence Zone (ITCZ) (Liu et al. 2020; Moreno-Chamarro et al. 2020), the Indian Monsoon (Zhang

and Delworth 2006), and the El-Niño Southern Oscillation (Timmermann et al. 2007). Changes to the AMOC mean state resulting from anthropogenic climate forcing thus have the potential to transform the global climate system (e.g., Vellinga and Wood 2002; Zhang and Delworth 2005; Jackson et al. 2015; Liu et al. 2020; Bellomo et al. 2021). Whilst strong efforts have been directed towards understanding the near-term transient response of the AMOC, the nature of, and the mechanisms influencing its equilibrium response to climate change remain poorly understood and are the focus of the present study.

# 1.1 Transient response and AMOC collapse

Idealized models, general circulation models (GCMs), and paleoclimate studies have evidenced two distinct states of AMOC, sometimes referred to as the on- and off- states (e.g., Stommel 1961; Rooth 1982; Manabe and Stouffer 1988; Dansgaard et al. 1993; Rahmstorf 1995; Bohm et al. 2015;

Published online: 06 April 2024



Paul Edwin Curtis paul.curtis@yale.edu

Department of Earth and Planetary Sciences, Yale University, New Haven, CT, USA

LOCEAN/IPSL, Sorbonne University, Paris, France

for a recent review see Weijer et al. 2019). The present-day 'active' circulation is characterized by northward mass transport in the upper ocean, deep water formation in the Subpolar North Atlantic (SPNA) (e.g., Speer and Tziperman 1992; Marshall and Schott 1999), and a strong overturning circulation (e.g., Warren 1983; Killworth 1983; Frajka-Williams et al. 2019; Trenberth et al. 2019).

Conversely, the off- state of circulation is distinguished by markedly reduced rates of deep water formation in the SPNA, and reduced northward mass and heat transports. A rapid transition into this state may eventuate if, for example, surface freshwater fluxes into the region become large enough to 'shut off' deep water formation by increasing the stability of the water column. Such an AMOC collapse is a well-studied tipping point (i.e., a bifurcation point) (e.g., Stommel 1961; Manabe and Stouffer 1993, 1995; Rahmstorf 1995, 2002; Fedorov et al. 2007; Barreiro et al. 2008; Lenton et al. 2008; Hofmann and Rahmstorf 2009; McKay et al. 2022). One should note here that these terms, on- and off- states imply equilibrium states. Hence, if a transient offstate of the AMOC develops, sufficiently long computations may be required to follow its long-term evolution to equilibrium and to establish whether the AMOC will recover or stay collapsed (e.g., Stouffer and Manabe 2003; Gent 2018; Bonan et al. 2022) and whether a true bifurcation point has been reached. In fact, in a recent review, Gent (2018) has suggested that a true AMOC bi-stability is reduced in fullycoupled models simulating the present-day climate, although a transient "off-" state may persist for several hundreds or thousands of years after a strong climate forcing.

Paleoclimate studies suggest that transitions between the two states of overturning circulation occurred in the past with significant consequences for climate, possibly induced by freshwater forcing in the North Atlantic (Broecker et al. 1985; Dansgaard et al. 1993; Barker et al. 2009; Bohm et al. 2015). In addition, in glacial climates, the increasing presence of sea ice in the Southern Ocean during (austral) summer (e.g., Ferrari et al. 2014) may have resulted in stronger negative buoyancy forcing in the surface ocean around Antarctica, leading to an increased volume of Antarctic origin waters in the North Atlantic, and ultimately a shoaling of the NADW cell of the AMOC (see also Marzocchi and Jansen 2017, and the earlier study of Shin et al. 2003). Several competing factors may have influenced the AMOC mean state on longer geological timescales, from changing atmospheric CO<sub>2</sub> concentrations (Rohling et al. 2012; Zhang et al. 2017) to topographical changes and sea-way openings (Brierley and Fedorov 2016) Overall, this poses paleoceanographers with a complicated problem to disentangle.

In the context of modern climate change, several processes linked to anthropogenic greenhouse gas emissions may reduce the rates of deep water formation in the near future and could lead to AMOC weakening and a potential collapse. These processes include both the warming and freshening of the upper ocean (due to Arctic sea ice melting, and melting of the Greenland ice sheet, e.g., Sévellec et al. 2017; Liu et al. 2019; Ackermann et al. 2020; Li et al. 2021a, b). Nevertheless, although AMOC weakening may arguably be already detected in observations (Caesar et al. 2018; Boers 2021), large uncertainties persist due to strong natural variability of the circulation (Moat et al. 2020; Jackson et al. 2022).

CMIP models generally predict significant weakening of the AMOC under greenhouse gas forcing by 2100, although an AMOC collapse is currently not expected during this century (Gregory et al. 2005; Stouffer et al. 2006; Weaver et al. 2012; Cheng et al. 2013; Weijer et al. 2020), unless the current generation of climate models overestimate AMOC stability (Liu et al. 2017). Obfuscating model predictions, there remains a large inter-model disagreement on the magnitude and timing of the projected weakening (Weijer et al. 2020), and more fundamentally, on various properties of the AMOC mean state itself (e.g., Danabasoglu et al. 2014; Huezé 2017, 2021).

## 1.2 Equilibrium response and AMOC recovery

AMOC recovery describes the gradual transition from inactivity into a state of active overturning (e.g., Manabe and Stouffer 1993; Stouffer and Manabe 2003). This process is far less discussed, typically because it occurs on significantly longer timescales after the circulation has initially collapsed. It is also dependent on the nature of the imposed forcing—freshwater versus radiative forcing. The latter may allow a full AMOC recovery, as the thermal structure of the ocean gradually adjusts. The former would typically require a reduction in the freshwater forcing and the system being mono-stable (e.g., Weijer et al. 2019).

More directly, evaluating AMOC recovery with GCMs in response to radiative forcing is made notably difficult due to the long timescales necessary for an equilibrium, or quasi-equilibrium state to be reached (Stouffer 2004). Indeed order  $10^3$ – $10^4$  year-long simulations are usually required to capture a total, or even partial recovery in circulation strength (Manabe and Stouffer 1993; Stouffer and Manabe 2003; Zhu et al. 2015; Bonan et al. 2022). This analysis is further compounded by difficulties in isolating mechanism for recovery in the presence of strong coupling and several competing climate feedbacks (Jackson 2013).

In one of the earliest studies of its kind, Manabe and Stouffer (1993) (and its follow-up Stouffer and Manabe 2003) attributed the eventual AMOC recovery in their GCM to enhanced subsurface warming (also discussed in Wiebe and Weaver 1999) which slowly enhances the meridional buoyancy gradient throughout the North Atlantic. The authors further discussed the role of deep ocean warming



in eroding the notable stratification introduced by freshwater fluxes at the SPNA. However, their analysis is rarely revisited, and accordingly, the role of other mechanisms involved in the AMOC's equilibrium response remain poorly understood.

A recent study by Bonan et al. 2022 examined seven models with abrupt 4xCO<sub>2</sub> experiments submitted as part of LongRunMIP (Rugenstein et al. 2019), with integration lengths ranging from 1000 to 5900 years. Across these models, the initial collapse to the AMOC occurs on multi-decadal/ centennial timescales. Their study concluded that AMOC recovery results from two concurrent processes. The first is a thermally-driven recovery to the meridional density gradient, which is traditionally believed to be an important driver of the AMOC, e.g., Stommel 1961 (although this must be considered in conjunction with the depth of the NADW cell if used directly as a diagnostic of changes to the AMOC; de Boer et al. 2010; Bonan et al. 2022). The second is the erosion of high latitude North Atlantic vertical stratification by slowly increasing upper ocean salinity. Consistent with a stronger North Atlantic freshening and enhanced stratification during the AMOC weakening phase, Bonan et al. 2022 determined that models with a stronger loss of sea ice exhibited a weaker AMOC recovery, which is consistent with the studies of Li and Fedorov (2021) and Li et al. (2021a, b). Several limitations of their study include integration lengths which are too short for most of the models used (only 2-3 models appear to reach a quasi-equilibrium by the end of integration), and only one type of CO<sub>2</sub> forcing is considered (4xCO<sub>2</sub>).

Instead, simulations which artificially freshen the SPNA (without radiative forcing), known as "freshwater hosing", are more often considered (e.g., Stouffer et al. 2006; Jackson 2013; Haskins et al. 2019; Thomas and Fedorov 2019). If the AMOC has not completely collapsed, and the freshening continues, these studies typically show a multicentennial partial AMOC recovery after the initial reduction (e.g., Thomas and Fedorov 2019), although not in all studies (e.g., Mecking et al. 2016; see also Jackson et al. 2023). Here, the mechanisms for AMOC recovery include the salinity advection feedback (e.g., Jackson 2013; Cheng et al. 2018), in which the (weakened) AMOC slowly advects relatively saline surface waters from low latitudes, simultaneously increasing surface density/reducing stability at high latitudes. However, these studies cannot capture the crucial influence of ocean ventilation on deep ocean warming expected for higher CO<sub>2</sub> concentrations (de Boer et al. 2007).

# 1.3 Motivation

In this paper we evaluate the response of the AMOC on equilibrium timescales to an abrupt radiative forcing using the Community Earth System Model (CESM) (Gent et al. 2011; Shields et al. 2012) in its relatively coarse configuration. The model used here means that we can capture more accurately the influence of feedbacks throughout the climate system, but still conduct long climate simulations. In effect, here we are revisiting and extending the early study of Manabe and Stouffer (1993); see Methods.

We consider characteristics of the AMOC mean state and quantify the model's equilibrium in Sect. 3. We specifically assess the winter mixed layer, in conjunction with the three-dimensional density structure (schematized in Fig. 1) to diagnose the evolution of the AMOC. Following this, we discuss potential mechanisms for AMOC recovery, focusing on changes to the thermohaline structure of the North Atlantic Ocean in Sect. 4. In Sect. 5 we discuss the AMOC response to global cooling. Finally, the results are placed in broader context in Sect. 6.

# 2 Methods: model configuration, experimental set-up, and key metrics

For this study we run CESM version 1.0.4 (provided by the National Centre for Atmospheric Research) in a low resolution gx3v7 configuration with T31 spectral truncation, appropriate for multimillennial climate simulations. This fully-coupled model uses the parallel ocean program version 2 (POP2) with 60 vertical levels and a maximum nominal spacing of  $\sim 3^{\circ}$ , decreasing to  $\sim 0.5^{\circ}$  close to the equator and at high latitudes in the Northern Hemisphere. The atmospheric component is the Community Atmosphere Model version 4 (CAM4) which is solved spectrally at T31

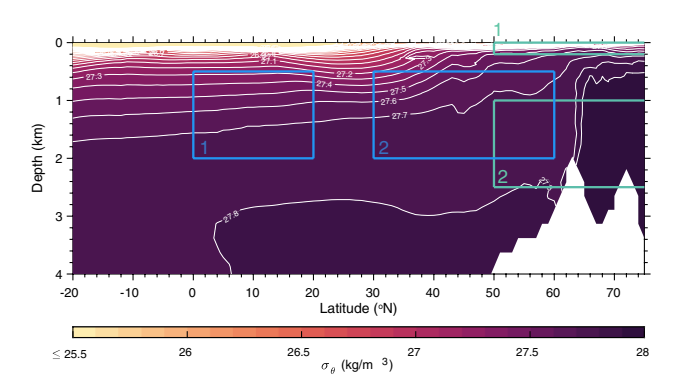


Fig. 1 Schematic for density metrics presented in Figs. 2b and 3a. Color shading shows zonally averaged  $(60^{\circ}\text{W} \leq \varphi \leq 0^{\circ}\text{W})$  potential density (referenced to the surface) anomaly (relative to  $1000 \text{ kg/m}^3$ ) in the North Atlantic. The meridional density gradient computed in Fig. 2b is the difference in potential density averaged over blue box '2' and blue box '1'. Stratification computed in Fig. 3a is the difference in potential density averaged over green box '2' and green box '1'; the vertical salinity and potential temperature gradients used in Fig. 3b and c are computed likewise



8000

truncation (corresponding to a  $3.75^{\circ} \times 3.75^{\circ}$  nominal horizontal grid resolution) with 26 vertical levels. The ice model is NCAR's Community Ice Code, and the land component is the Community Land Model.

To analyze the response of the AMOC to a range of radiative forcing scenarios, we perform a pre-industrial control (piControl; 284.7 ppm) run in addition to abruptly forced experiments with atmospheric concentrations of 0.5xCO<sub>2</sub>, 2xCO<sub>2</sub>, 4xCO<sub>2</sub>, 8xCO<sub>2</sub>, and 16xCO<sub>2</sub> relative to the preindustrial climate. Here, atmospheric CO<sub>2</sub> concentrations are step increased (decreased for 0.5xCO<sub>2</sub>) to the prescribed level at the start of integration and held constant for the duration. Each integration is initiated from a 769-year spinup run using pre-industrial control conditions; the initial portion of the global warming scenarios are described in Fedorov et al. 2015. We have attempted to run each experiment towards an equilibrium (c.f. Table 1), however the abrupt 16xCO<sub>2</sub> experiment is limited to 4250 years due to a violation of the model's equation of state for seawater (salinity exceeds an allowed critical value). The 8xCO2 experiment is the longest warming experiment with 10,000 years of computations, but even then, we are unable to conclude confidently whether an equilibrium has been reached. The 0.5xCO<sub>2</sub> experiment is run for 6250 years and appears to remain in a state of weak overturning as the experiment approaches equilibrium.

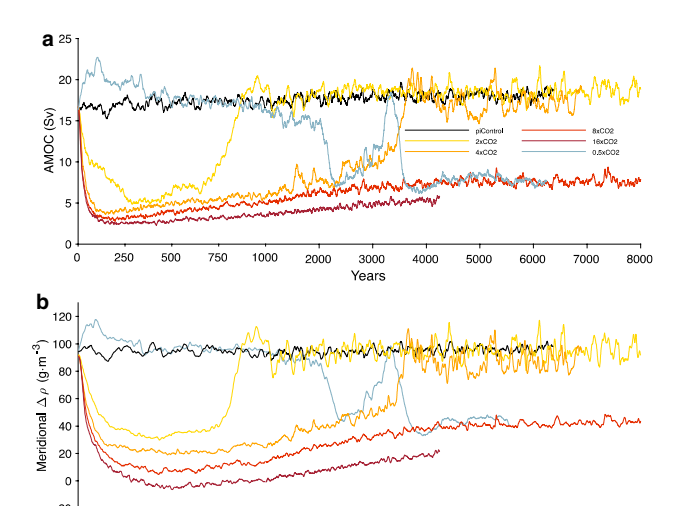
In summary, our general modelling approach is similar to Stouffer and Manabe (2003), but we run longer simulations and include the  $8xCO_2$  and  $16xCO_2$  experiments. We stress that the model here does not use salinity flux adjustment, which may influence the stability of the AMOC (e.g., Yin and Stouffer 2007; Gent 2018).

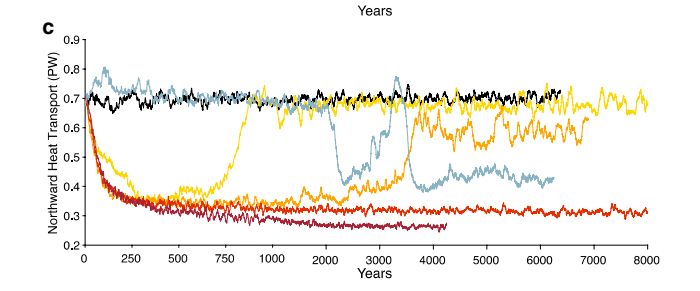
First, to quantify the strength of the AMOC, we compute the maximum zonally averaged Eulerian streamfunction in the North Atlantic, presented in Fig. 2a. To retain the density driven circulation signal and avoid the low-latitude wind-driven overturning cell (subtropical cells,

**Table 1** Summary of model experiments and respective integration time

Experiment	Years of Integration
$0.5xCO_2$	6250
piControl	6375
$2xCO_2$	8172
$4xCO_2$	6895
$8xCO_2$	10,000
16xCO <sub>2</sub>	4250

We define the transient time period (T) as years 300–600 for all experiments; the equilibrium time period is defined as the last 1000 years of each model's integration time





3000

Fig. 2 a Maximum Eulerian streamfunction in the North Atlantic basin (1  $Sv = 10^6 m^3 s^{-1}$ ) showing the AMOC strength. **b** Meridional density difference between low latitudes and midlatitudes in the North Atlantic, i.e. the area-weighted and depth-averaged PD difference between blue box '2' and blue box '1' in Fig. 1. **c** Maximum Eulerian-mean northward heat transport (1PW= $10^{15}$ W) in the North Atlantic basin. **a–c** A 10-year running mean is applied over the first 1000 years, and a 25-year running mean is applied thereafter. Note, that hereafter we use two different linear scales for the time axis—before and after the first 1000 years

STC, e.g., McCreary and Lu 1994), we constrain our metric to find the maximum below z = 750 m and north of 30°N. To provide further insight into the simulated AMOC weakening, we briefly consider the density structure of the Atlantic Ocean. In idealized models, the Eulerian streamfunction and hence the circulation flow rate can be related to the meridional density (buoyancy) gradient (e.g., Stommel 1961), as well as to wind stress in the Southern Ocean (Gnanadesikan 1999; Sévellec and Fedorov 2011; Nikurashin and Vallis 2012). Hence, we compute the meridional density difference between the tropics  $(60^{\circ}\text{W} \le \phi \le 0^{\circ}\text{W}; 0^{\circ} \le \theta \le 20^{\circ}\text{N}; 0.5 \text{ km} \le z \le 2 \text{ km}) \text{ and}$ midlatitudes (30°  $\leq \theta \leq 60$ °N; same  $\phi$ , z domain), shown in Fig. 2b. Consistent with previous studies of the AMOC, we find a tight relationship between the maximum AMOC and the magnitude of meridional density gradient between high and low latitudes of the North Atlantic.



As discussed in the introduction, the rapid collapse of the AMOC is primarily driven by surface buoyancy forcing in the SPNA region, which increases vertical stratification and suppresses dense water formation. To quantify this, we define the SPNA as  $60^{\circ}\text{W} \le \phi \le 60^{\circ}\text{E}$ ,  $50^{\circ}\text{N} < \theta < 75^{\circ}\text{N}$  (which has been chosen to include the region of deep convection), and then compute the density difference between the deep ocean (1 km  $\leq$  z  $\leq$  2.5 km) and upper ocean (0 m  $\leq$  z  $\leq$  200 m), presented in Fig. 3a (see Fig. 1 for a schematic). Thermal and haline contributions to the stratification are presented in Fig. 3b, and c, respectively; in this model the stratification is dominated by the haline contribution (c.f. Figure 3c). We approximate the vertical density difference using a linearized equation of state, in which  $\alpha$  and  $\beta$  are the column averaged coefficients of thermal expansivity and haline contraction, respectively, computed using the TEOS-10 equation of state for seawater;  $\rho_0 = 1025 \text{ kg/m}^3$  is a reference density.

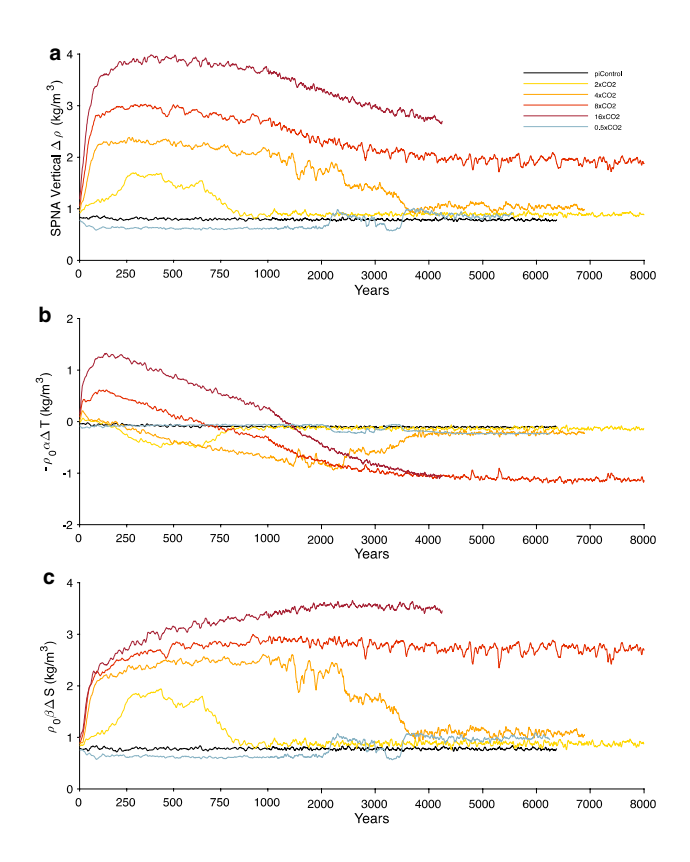
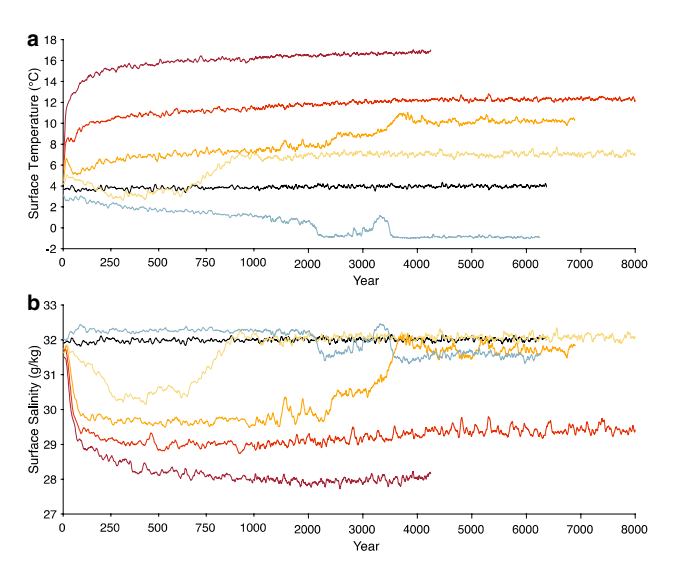


Fig. 3 a Mean vertical stratification in the subpolar North Atlantic (SPNA) computed as a density difference between the upper ocean and deep ocean (see also Fig. 1). **b**, **c** Thermal and haline contributions to stratification in the SPNA. The vertical density difference is approximated by a linearized equation of state (i.e.,  $a \approx b+c$ ) in which  $\alpha$  and  $\beta$  are the SPNA column averaged coefficients of thermal expansivity and haline contraction, respectively. **a–c** A 10-year running mean is applied over the first 1000 years, and a 25-year running mean is applied thereafter; note that in **b** and **c** positive values indicate a positive contribution to the bulk stratification

Therefore, summing thermal and haline contributions (approximately) yields the density difference.

We provide further context on the surface thermohaline response in Fig. 4, which plots SPNA area-weighted SST (Fig. 4a) and sea surface salinity (SSS) (Fig. 4b). The surface response is discussed in more detail in Sect. 4.1; the role of the deep ocean is discussed in Sect. 4.2.

Finally, to quantify more general aspects of the model's approaching equilibrium, we consider globally averaged top of the atmosphere (TOA) radiative imbalance as a time series for all experiments in Fig. 5a, calculated as the incoming short-wave radiation  $(F_{ISW})$  minus outgoing longwave radiation  $(F_{OLR})$ . The area under each curve is therefore a direct measure of the energy gained by the climate system (per unit area). Figure 5a indicates the climate is not close to a radiative equilibrium in any scenario during the first 1000 years, and a true radiative equilibrium appears to be reached after about 5000 years (a little sooner for 2xCO<sub>2</sub>). At early times, Fig. 5a also illustrates that the initial radiative imbalance increases linearly with each doubling of atmospheric CO<sub>2</sub> (e.g., Etminan et al. 2016), and decreases (approximately) exponentially in time. Figure 5b and c plot globally averaged surface ocean temperature (highest grid level), and globally averaged deep ocean temperature at 3 km (nearest grid level), respectively. Critically, even after the atmospheric radiative equilibrium is reached, ocean temperature (and salinity) continues to adjust in several experiments (Fig. 5b, c).



**Fig. 4** Area weighted (**a**) sea surface temperature (SST) and (**b**) sea surface salinity (SSS) in the SPNA for all experiments. **a**, **b** A 10-year running mean is applied over the first 1000 years, and a 25-year running mean is applied thereafter. See Methods for the definition of the SPNA



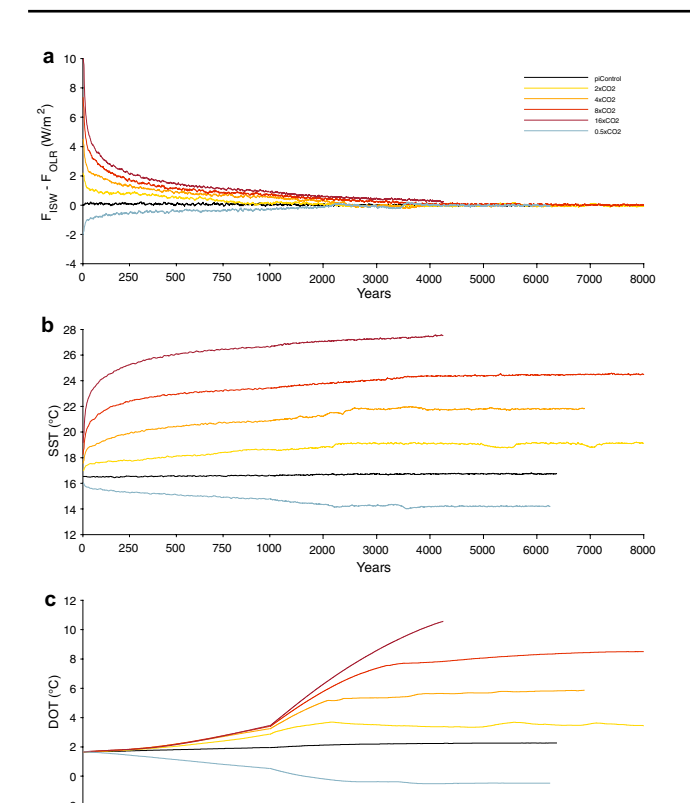


Fig. 5 Metrics to quantify the system's transition to the state of equilibrium in the experiments: a globally averaged top of the atmosphere (TOA) radiative imbalance; b globally averaged sea surface temperature (highest ocean grid level); and c globally averaged deep ocean temperature (DOT) at 3 km depth (nearest grid level). a–c A 10-year running mean is applied over the first 1000 years, and a 25-year running mean is applied thereafter. The two different linear scales used for the time axis before and after the first 1000 years explain the kink in some of the profiles in c. Note that even after the model reaches TOA radiative equilibrium, temperatures in the deep ocean may still be changing

3000

8000

7000

### 3 Evolution of the AMOC

500

#### 3.1 AMOC collapse and subsequent recovery

As we abruptly increase atmospheric  $CO_2$  concentrations, a rapid collapse of the AMOC strength occurs in all warming experiments. The minimum in overturning is reached during the first 100-250 years and occurs more rapidly for larger forcing. By contrast, the  $0.5 \text{x} CO_2$  experiment increases by  $\sim 5$  Sv to reach a maximum in strength over the same period, which precedes a very gradual decline of nearly 10 Sv over the next 2000 years. This slow decline is followed by a much faster collapse of the MOC. The circulation then recovers, leading a second collapse  $\sim 1500$  years after the first, potentially resembling a Dansgaard-Oeschger oscillation (e.g., Peltier and Vettoretti 2014; Klockmann et al. 2018). The abrupt  $0.5 \text{x} CO_2$ 

**Table 2** For all global warming scenarios, a summary of timescales (in years) for (i) the initial AMOC weakening phase (middle column), and (ii) the eventual recovery of the AMOC (last column)

Experiment	Maximum Weaken- ing	Recovery
2xCO <sub>2</sub>	306	887
$4xCO_2$	169	3619
$8xCO_2$	203	> 10,000 years, or never
16xCO <sub>2</sub>	221	Inconclusive

The weakening timescale is defined as the minimum AMOC strength in each of the (smoothed) time series shown in Fig. 2a. The recovery timescale is defined as the first year in which the AMOC overshoots the piControl for the  $2xCO_2$  and  $4xCO_2$  experiments

experiment will be discussed briefly in Sect. 5, and in more detail in a later publication. From here on, we focus on the pre-industrial control and the four global warming experiments.

In all warming experiments, after the AMOC minimum is reached, the circulation stays in a collapsed state for hundreds, or thousands of years depending on the magnitude of the forcing. In the abrupt 2xCO<sub>2</sub> experiment, we observe a rapid and full recovery of the AMOC after ~ 900 years. The circulation remains stable in this actively overturning mode until the end of integration. An AMOC recovery also occurs in the 4xCO<sub>2</sub> experiment, but after ~ 3600 years. Timescales for AMOC weakening and recovery are summarized in Table 2 and discussed in Sect. 6. In our 8xCO<sub>2</sub> experiment, even after 10,000 years the AMOC has not recovered. In the last case, since the deep ocean is still warming (albeit incredibly slowly) in the global mean towards the end of integration (Fig. 5c), it is therefore feasible that an AMOC recovery may happen after further (but likely extensive) integration of this experiment.

We briefly note the timescales here are longer than the AMOC recoveries discussed in the abrupt 2xCO<sub>2</sub> (after 600 years) and 4xCO<sub>2</sub> (after 1750 years) experiments in Stouffer and Manabe (2003). Moreover, the multi-model study of Bonan et al. 2022 used a higher resolution version of CESM1.0.4 with abrupt 4xCO<sub>2</sub> forcing. In their study, the AMOC recovers somewhat faster (after ~ 1000 years), as compared to our 4xCO<sub>2</sub> experiment (~3600 years), and even overshoots. This is likely related to a too strong AMOC in their model configuration (about 25 Sv for the piControl versus 17 Sv in the present study; compare to estimates of ~ 17 Sv from the RAPID array, e.g., Frajka-Williams et al. 2019). The AMOC is also more stable in their model to external perturbation (Li et al. 2021a, b). More generally the AMOC overshoot sometimes observed in GCMs (Stouffer and Manabe 2003; Bonan et al. 2022), hosing studies (e.g., Jackson 2013; Haskins et al. 2019), and more idealized models (e.g., Jansen et al. 2018) is absent in our results, and, if



any, is masked by variability (see also the study of Sigmond et al. 2020).

Considering Figs. 2, 3, 4, 5 together, for the subsequent analysis we conditionally define the transient period (T) of AMOC response as years 300–600 for all experiments to capture the dynamics when the overturning circulation is in the collapsed state for all warming experiments, and when the TOA radiative imbalance is still notable. The equilibrium or quasi-equilibrium period (E) is taken as the last 1000 years of each run (see Table 1).

Consistent with the theoretical expectations, across all experiments we observe a strong correlation between changes in the meridional density gradient (Fig. 2b), the northward mass flux implied by Fig. 2a, as well as the maximum meridional heat transport (Fig. 2c). Although all abrupt  $CO_2$  increase experiments are at  $\leq 5$  Sv in strength at absolute minimum, we note that the circulation remains northward, in agreement with LongRunMIP abrupt  $4xCO_2$  model experiments (Bonan et al. 2022), and in contrast to the earlier study of Stouffer and Manabe (2003). Figure 1b demonstrates that at this depth, the midlatitude ocean remains marginally denser than lower latitudes, in agreement with the still weakly northward circulation when the AMOC is around its minimum value.

On the same timescale as AMOC collapse, a marked increase in vertical stratification is observed in Fig. 3a, implying reduced rates of NADW formation, and overturning, since surface waters are no longer dense enough to penetrate into the deeper ocean. Figures 6, 7 shows that

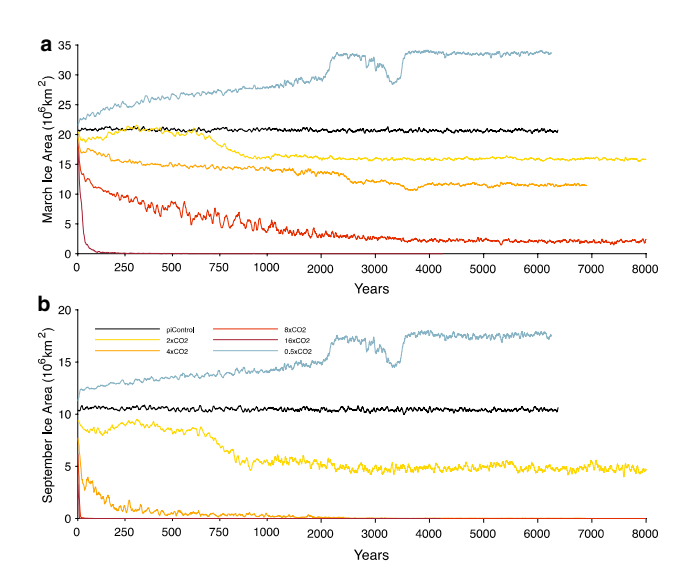


**Fig. 6** a March, and **b** September Arctic total sea ice area. Here, sea ice area is calculated as the ice area fraction per grid cell multiplied by the grid cell area. **a, b** A 10-year running mean is applied over the first 1000 years, and a 25-year running mean is applied thereafter. Arctic sea ice disappears in the  $16xCO_2$  experiment after the first 100 years

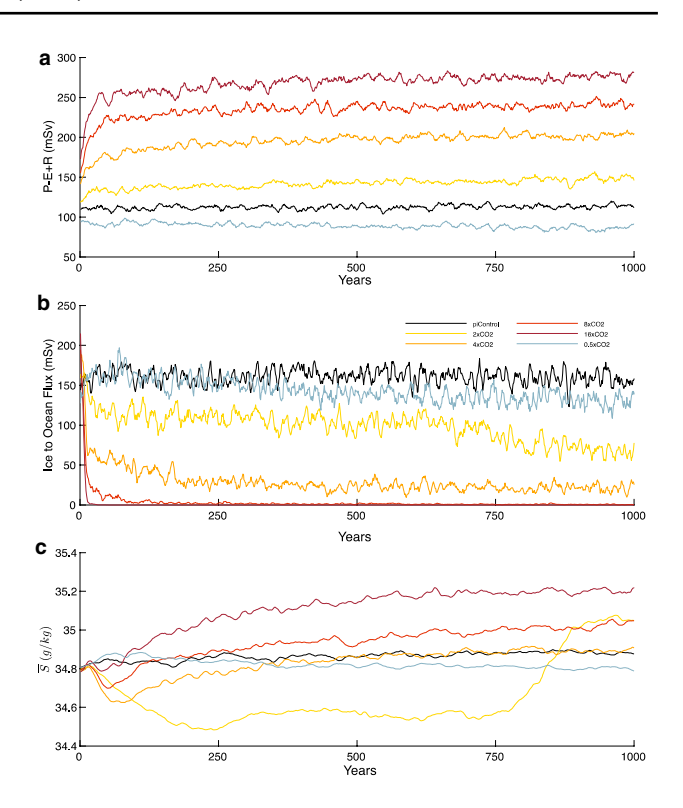
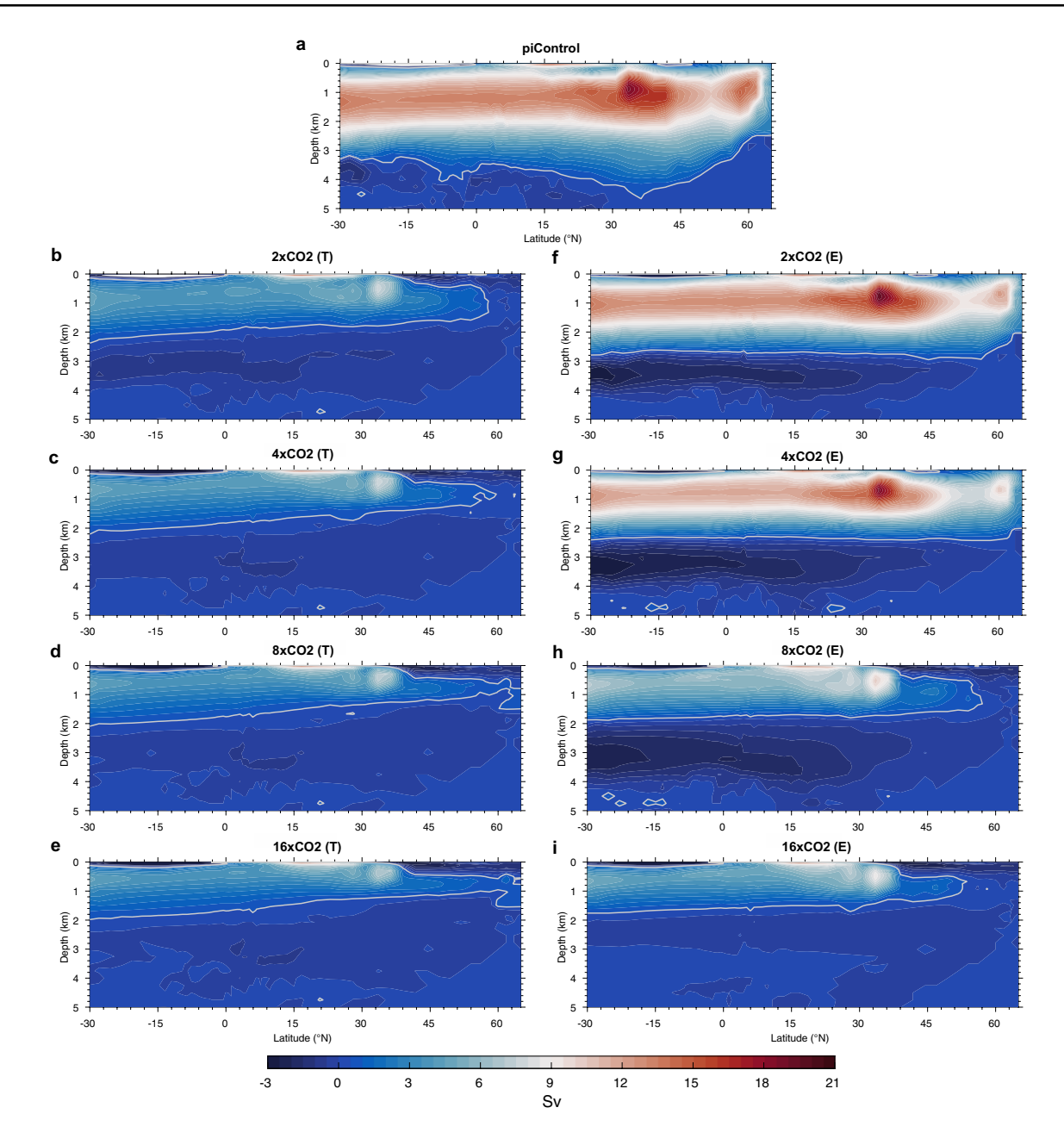


Fig. 7 Contributions to salinity changes in the SPNA from (a) the atmospheric hydrological cycle (P - E + R) is the surface integrated precipitation—evaporation+land runoff fresh water flux), **b** melting sea ice and brine rejection, and **c** volume mean salinity in the upper 2000 m over the SPNA region. Here, we only present the first 1000 years of data. Fluxes are shown in units of mSv of freshwater. **a**–**c** A 10-year running mean is applied to all time series

initially following the forcing (first 10 years) this is due to enhanced sea ice melt; as sea ice recedes, freshening due to the hydrological cycle (P-E+R) becomes the dominant source of surface freshening in the SPNA beyond the first ~ 25 years. Ocean vertical stratification in the SPNA is further enhanced by comparatively higher rates of warming in the upper ocean against the deep ocean (c.f. Figures 3b, 5b and c; also, Mikolajewicz and Voss 2000). Although the simulated climate response is different in this model than in experiments which only freshen high latitude waters, both the timescales and magnitudes of AMOC weakening discussed in Haskins et al. (2019) for instance are comparable to this study, confirming that surface buoyancy adjustments are driving AMOC collapse. We discuss the surface response in more detail in Sect. 4.1.

To evaluate changes in the two-dimensional structure of the AMOC, we show zonally averaged snapshots of the Eulerian streamfunction in the z-coordinate in Fig. 8. In the control simulation (Fig. 8a) the AMOC cell is maximum around 35°N and 1 km depth and extends below 3 km depth. The spatial domain used to calculate the meridional density contrast plotted in Fig. 2b has been chosen to pick





**Fig. 8** Zonally-averaged streamfunction in the North Atlantic latitude-depth plane; the streamfunction includes the Eulerian, bolus, and sub-mesoscale components. **a** Data for the last 1000 years of preindustrial control data as a reference. Abrupt 2xCO<sub>2</sub>, 4xCO<sub>2</sub>, 8xCO<sub>2</sub>, and 16xCO<sub>2</sub> experiments: **b**-**e** data is averaged for the transient time period; **f**-**i** data is averaged over the equilibrium time period. The

grey contour, set at 0.5 Sv, is used to indicate the approximate depth of the AMOC cell. Hereafter, T and E refer to averages over the transient (years 300–600) and equilibrium intervals (the last 1000 years of the experiments), respectively, see Methods. **f–h** Note the shoaling of the NADW cell relative to the pre-industrial control, and the strong intrusion of AABW

out this streamfunction maximum. A secondary circulation maximum is observed towards the SPNA, which is associated with high latitude overturning. When the AMOC has collapsed (Fig. 8b–e), the NADW cell is visibly weakened across all latitudes and now extends to a shallower depth of ~1.5 km. We note that some residual AMOC present in Fig. 8b–e is due to the inclusion of the Eulerian-mean

streamfunction in the z-coordinate, which retains the influence of the North Atlantic subtropical gyre.

Serving as a proxy to assess the locations and rates of deep convection at high latitudes, the winter mixed layer depth (Fig. 9) indicates the location of deep convection and the depth to which surface waters can convect (e.g., Liu et al. 2019). The horizontal domain used in Fig. 3a



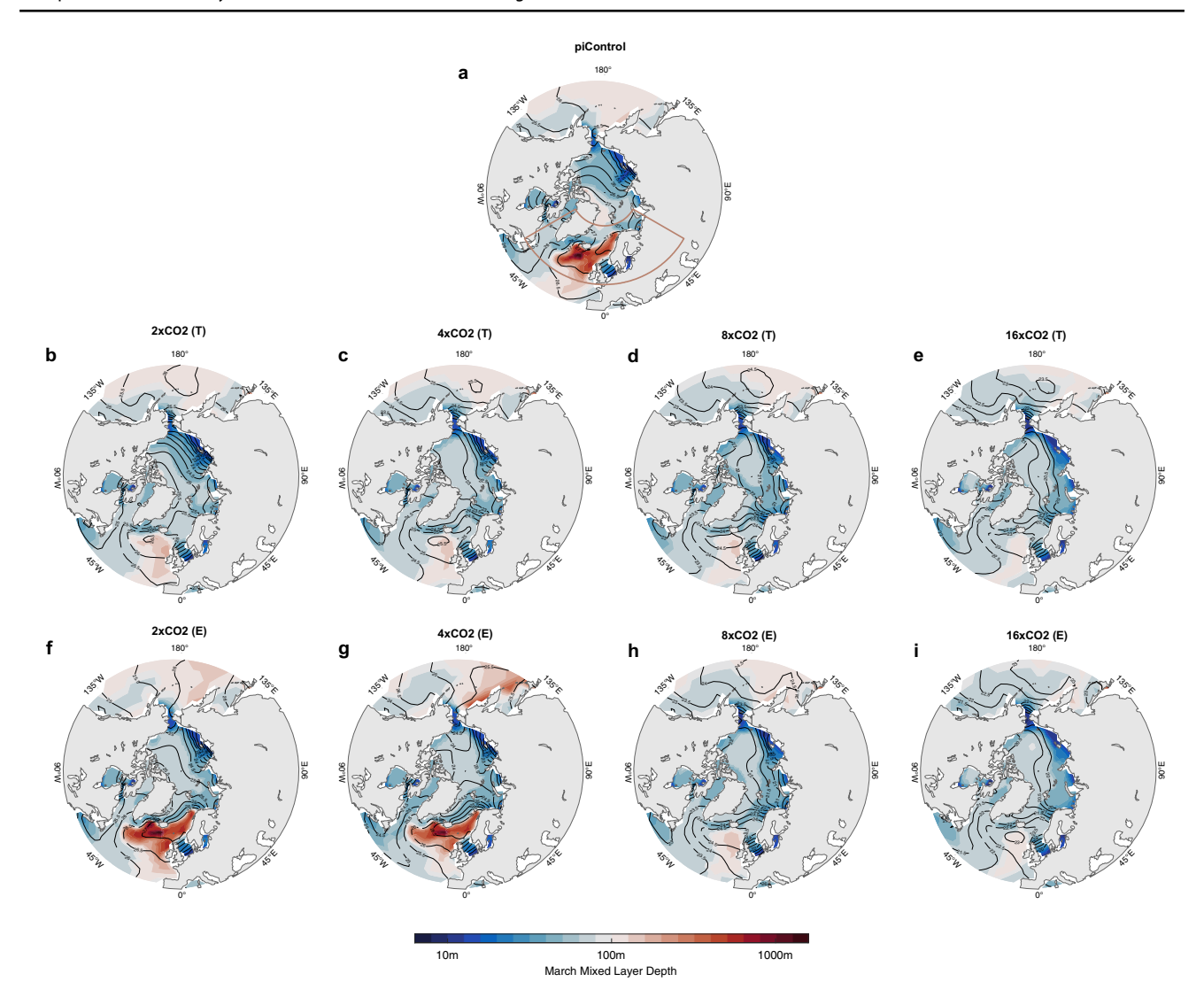


**Fig. 9** March mixed layer depth (MLD) over the Arctic and Subarctic regions (color shading) indicative of dense water formation. **a** Shows the last 1000 years of pre-industrial control data as a reference. Abrupt 2xCO<sub>2</sub>, 4xCO<sub>2</sub>, 8xCO<sub>2</sub>, and 16xCO<sub>2</sub> experiments: **b**–**e** data is averaged for the transient time period; **f**–**i** data is averaged over the

equilibrium time period. Note the logarithmic scale used for MLD. Black contours denote surface density anomalies relative to 1000 kg/  $m^3$ , averaged over the top 50 m of the ocean. Note the expansion of the mixed layer toward the Labrador Sea after the AMOC recovery in  ${\bf f}$  and  ${\bf g}$ 

has been chosen to include all regions in which strong overturning is implied by a deep MLD in the control state (i.e., the orange outline in Fig. 9a). The MLD becomes shallower following AMOC collapse, a consequence of the cessation in NADW formation. We note that the version of CESM we use does not produce deep water in the Labrador Sea, which is consistent with recent observations including those from the OSNAP array (e.g., Lozier et al. 2019; Chafink and Rossby 2019; Zhang and Thomas 2021; Li et al. 2021a, b) which suggest small contributions from this region to the AMOC, even though traditionally the Labrador Sea is considered an important region of deep water formation.

# 3.2 AMOC transition to equilibrium

We emphasize that adjustments within the deep ocean may continue to evolve for 10,000 years or even longer following the imposed climate forcing, even after a radiative equilibrium has been reached. Therefore, an absolute equilibrium may not be met in some of the abrupt forcing experiments until several tens of millennia of model integrations are performed (e.g., Jansen et al. 2018). We find that the deep ocean is evolving considerably in the  $16xCO_2$  experiment at the imposed end of model integration. Hence, given this, and the larger TOA radiative imbalance at the end of our model integration, we will



generally omit this forcing scenario from our discussion hereon in.

For both experiments in which the AMOC has recovered to pre-industrial strength, the AMOC cell is shallower than that in the control experiment (Fig. 8f and g), and the high latitude ocean has evolved into a marginally more stratified state (c.f. Figure 3a), coinciding with a shallower winter mixed layer depth. We note an intrusion of Antarctic Bottom Water (AABW) evident in Fig. 8f-h, which likely mutes the increase in North Atlantic deep water temperature. Overall, the structure of the meridional overturning in the Atlantic is somewhat different from the pre-industrial control, despite the 2xCO<sub>2</sub> and 4xCO<sub>2</sub> experiments reaching a similar maximum overturning strength. It is important that although the mixed layer has become shallower at equilibrium in these simulations, Figs. 9f and g illustrate a deepening of the mixed layer towards the Labrador Sea, which is related to a sea ice retreat off the Canadian and Greenland coasts.

In the 8xCO<sub>2</sub> experiment, several metrics including circulation strength, sub-Arctic stratification, and meridional density contrast have approximately stabilized by the end of integration. At this point the deep ocean temperature is also tending towards an equilibrium, but still marginally increasing. It is therefore possible that the large forcing has shifted the climate into a fundamentally different state in which high-latitude overturning is inhibited. However, surface salinity over the SPNA region keeps gradually increasing (Fig. 4b), and hence the possibility of a later AMOC recovery cannot be completely excluded.

Finally, a crucial climate property of the AMOC is its ability to transport heat to higher latitudes. However, the smaller meridional temperature gradients resulting from Arctic temperature amplification limit the oceanic meridional heat transport (MHT). Consistent with this, we find the equilibrium MHT associated with the recovered AMOC is weaker by  $\sim 0.025 PW$  for  $2xCO_2$ , and by  $\sim 0.1 PW$  for  $4xCO_2$  when compared to the control state (Fig. 2c), even though the AMOC mass transport is nearly the same.

# 4 The thermohaline response and AMOC recovery

Changes in temperature and salinity (i.e., the ocean thermohaline structure) are crucial in determining the mode of North Atlantic overturning, and more generally in setting the three-dimensional structure of North Atlantic circulation. As expected, response timescales of the deep ocean are much longer than those for the upper ocean (compare Fig. 5b and c). Consequently, we observe significant upper ocean temperature changes after < 100 years, whereas the deep ocean requires about 1000 years before a notable response in temperature is observed, and is still adjusting

after 5000 years and longer. Given the different response times between the upper and deep ocean evident in Fig. 5b and c, we discuss their respective responses in Sects. 4.1 and 4.2 to provide context to our discussion of potential mechanisms for AMOC recovery in Sect. 4.3.

# 4.1 Surface and upper ocean response

On transient timescales we observe a moderate to strong warming of the upper ocean (e.g., Fig. 4a); as expected, the magnitude of each response is larger with increasing initial radiative forcing. However, this warming is not spatially uniform. With the AMOC in a collapsed state, Fig. 10b-e shows a comparatively muted surface temperature response within the eastern SPNA (the region of deep water formation implied by Fig. 9) across all three experiments. For the case of an abrupt doubling of atmospheric CO<sub>2</sub> concentrations, Fig. 10b even demonstrates a moderate surface cooling in the eastern SPNA relative to the pre-industrial control. This phenomenon coincides with an increase in sea ice over the transient period for the 2xCO<sub>2</sub> experiment (Fig. 6). This behavior is likely due to the reduced northward MHT associated with AMOC collapse, in a which a so-called 'warming hole' develops (e.g., Kiel et al. 2020; Liu et al. 2020).

In the first few years following the abrupt forcing, strong global warming is enhanced in polar regions through the ice-albedo feedback, leading to a substantial and immediate reduction in sea ice cover (c.f. Figure 6). This dominates freshwater input to the SPNA for the first few years. Moreover, in response to global warming, an intensified northward atmospheric moisture transport through the midlatitudes is expected (Held and Soden 2006). This enhances precipitation at higher latitudes (Fig. 7a), thus further reducing surface density (salinity) in the SPNA (c.f. Figures 4b and 11) and hence transformation rates of surface waters into deep waters (e.g., Speer and Tziperman 1992). Figure 7 shows that freshening due to P - E + R is larger than the contribution from sea ice on timescales of decades and longer following the initial forcing; moreover, the contribution due to the hydrological cycle is towards the same order of magnitude as the entire freshening imposed in hosing experiments of Haskins et al. (2019). Both sea ice loss and enhanced P-E+R initiate a freshwater 'capping' (Stouffer and Manabe 2003) at high latitudes (obvious in Fig. 11), which is further enhanced through the positive salinity advection feedback. Figure 11 indicates that the reorganization in meridional atmospheric moisture transport and reduction in salinity advection concomitantly increases salinity at lower latitudes, which is retained in the North Atlantic subtropical gyre.

After the AMOC has recovered in the abrupt 2xCO<sub>2</sub> and 4xCO<sub>2</sub> experiments, surface waters in the SPNA are 4 °C to 7 °C warmer relative to the pre-industrial control. Increasing upper ocean temperature at high latitudes acts



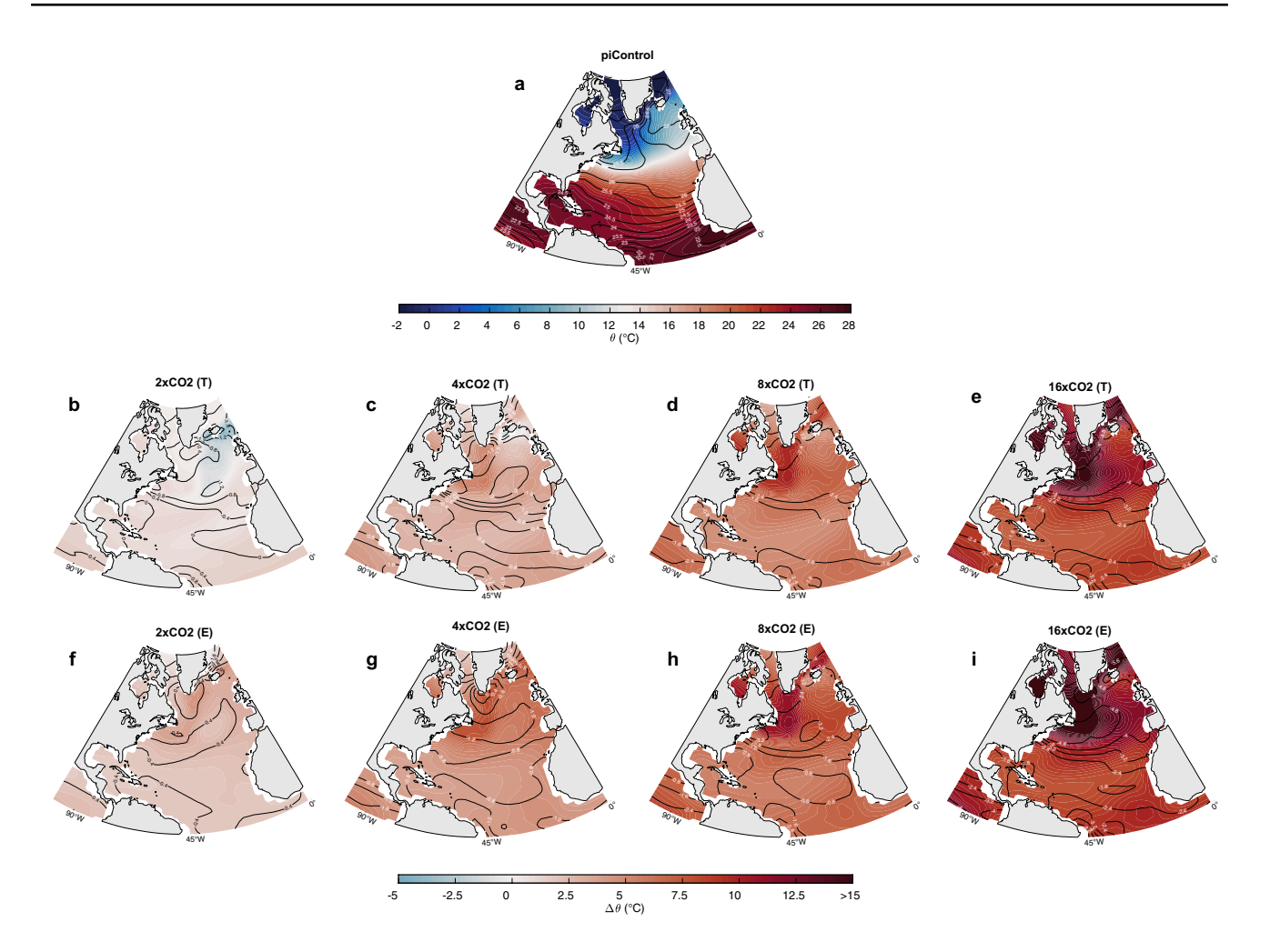


**Fig. 10 a** North Atlantic surface temperature averaged over the last 1000 years of pre-industrial control data. Black contours indicate potential density anomaly relative to 1000 kg/m³. **b–i** Surface ocean temperature anomalies relative to the pre-industrial Control for the

abrupt  $2xCO_2$ ,  $4xCO_2$ ,  $8xCO_2$ , and  $16xCO_2$  experiments. Data is averaged over the transient ( $\mathbf{b}$ - $\mathbf{e}$ ) and equilibrium time periods ( $\mathbf{f}$ - $\mathbf{i}$ ). Black contours indicate potential density relative to pre-industrial control

to decrease the surface density at equilibrium, potentially decreasing the surface area of transformable water and reducing rates of deep water formation. Furthermore, as the AMOC recovers here, there is a marked decrease in sea ice extent, attributable to a recovering northward MHT. The retreating winter sea ice around the Labrador Sea explains the deepening of the winter MLD at more westerly longitudes in the equilibrium state (c.f. Figures 6f and g), especially in the 4xCO<sub>2</sub> experiment. For this model we emphasize a control mean state cold bias which produces a very large ice coverage (see Fig. 9a, also see Shields et al. 2012). When this ice melts, a larger rate of surface temperature amplification occurs, thus further reducing surface density. This enhanced thermal response may contribute towards the longer AMOC recovery timescales in this model when compared to other GCM studies (Fig. 12).

#### 4.2 Deep and abyssal ocean response

Compared to the upper ocean, deep ocean thermohaline adjustments occur over much longer time periods, typically many thousands of years. Conceptually this can be quantified by the ideal ventilation age of the Atlantic Ocean, which is a measure of how long it takes for a water parcel near the surface to reach a particular location at depth. The ventilation age of the North Atlantic will grow significantly with AMOC in a collapsed state. This behavior is reflected in Fig. 13b—e and 14b—e in which there is very little change in temperature, salinity, and, therefore, density in the deep ocean (e.g., below 2 km) during the transient period. Conversely, on equilibrium timescales, at which point anomalies in temperature and salt have slowly diffused through the water column, the



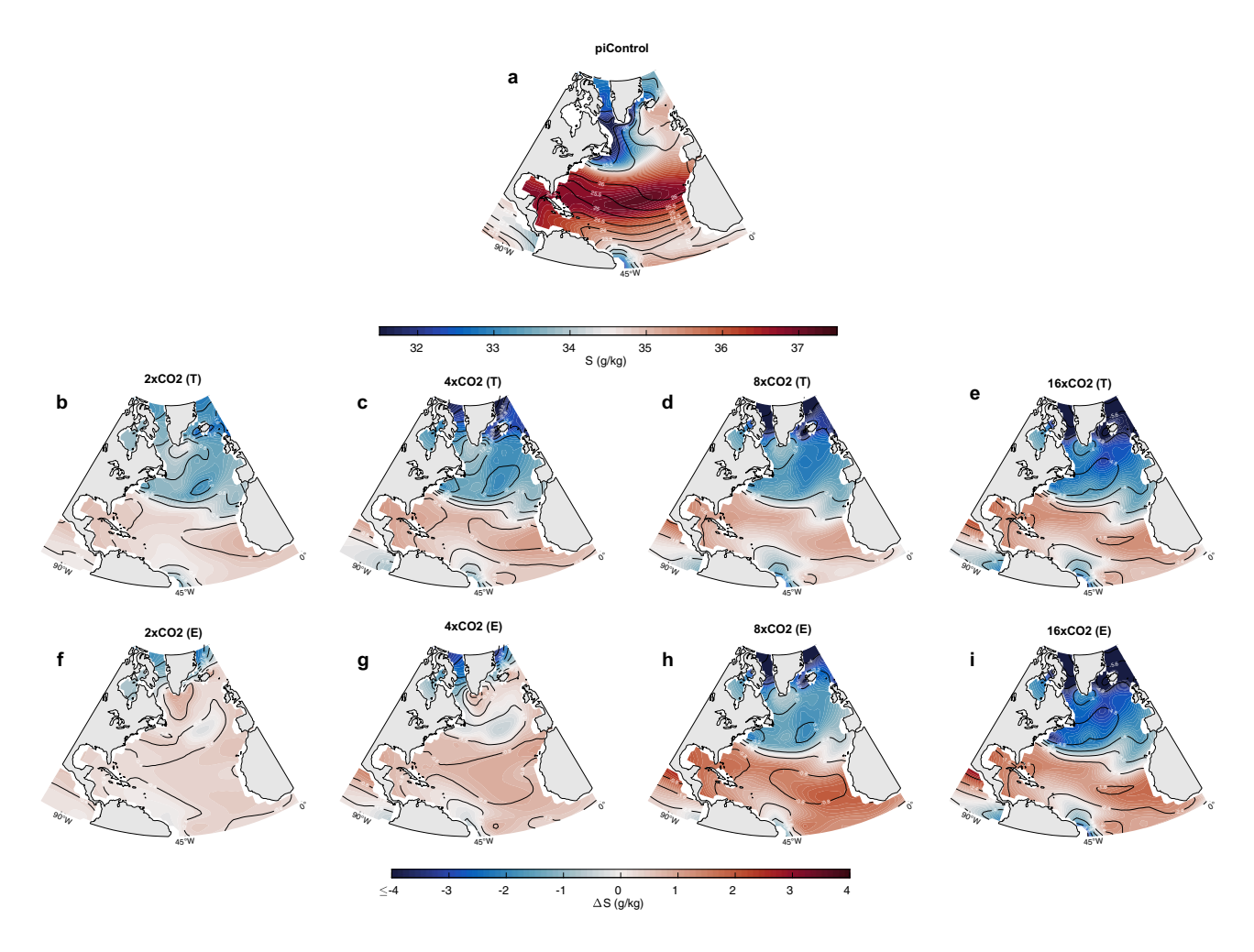


Fig. 11 As in Fig. 10 but for salinity. Note the pronounced transient freshening of the Arctic and Subpolar regions that is concurrent with AMOC collapse. This freshening persists in the 8xCO<sub>2</sub> and 16xCO<sub>2</sub> experiments through the end of integration

deep ocean response becomes much stronger (c.f. also Fig. 3c, for instance).

From theory, flatter isopycnals are observed in the ocean interior, but these bend towards the surface at northern high latitudes (where denser surface waters sink), and outcrop sharply at southerly latitudes in the Southern Ocean (due to wind-driven upwelling: Toggweiler and Samuels 1998; Gnanadesikan 1999; Marshall and Speer 2012; Haertel and Fedorov 2012; Nikurashin and Vallis 2012; Wolfe and Cessi 2014). Generally, when NADW formation is active, this density distribution gives rise to a meridional buoyancy gradient through the top 2 km of the Atlantic Ocean.

In the transient state, however, going from south to north across the North Atlantic basin the isopycnals have become flatter (and even crop down at higher latitudes) due to the high latitude freshening, and a cessation in NADW formation which usually brings denser water into the ocean interior. Ultimately, the meridional buoyancy gradient is eroded. However, when the AMOC has recovered, the isopycnal

surfaces again crop upwards at high latitudes due to a return to high NADW formation rates, although these surfaces are pushed slightly deeper at midlatitudes in the North Atlantic due to ocean warming; this is especially the case for the abrupt  $4xCO_2$  experiment. The meridional buoyancy gradient is restored in the top 2 km of the ocean, but to a marginally weaker state (c.f. Figure 2c).

During the transient time period when the AMOC is inactive, we note a strong increase in stratification across all latitudes south of 60°N. This does not extend to the abyssal ocean on transient timescales, which retains its characteristic low stratification. The potential density contours in Figs. 13b–e and 14b–e show that ocean stratification increases relative to the pre-industrial control on transient timescales. Despite an increase in salinity over the top 2 km of the ocean (Fig. 14b–e), which would otherwise act to reduce ocean vertical stratification, the large increase in temperature within the upper 2 km of the Atlantic Ocean compared to the deep ocean (Fig. 13b–e) must be responsible for



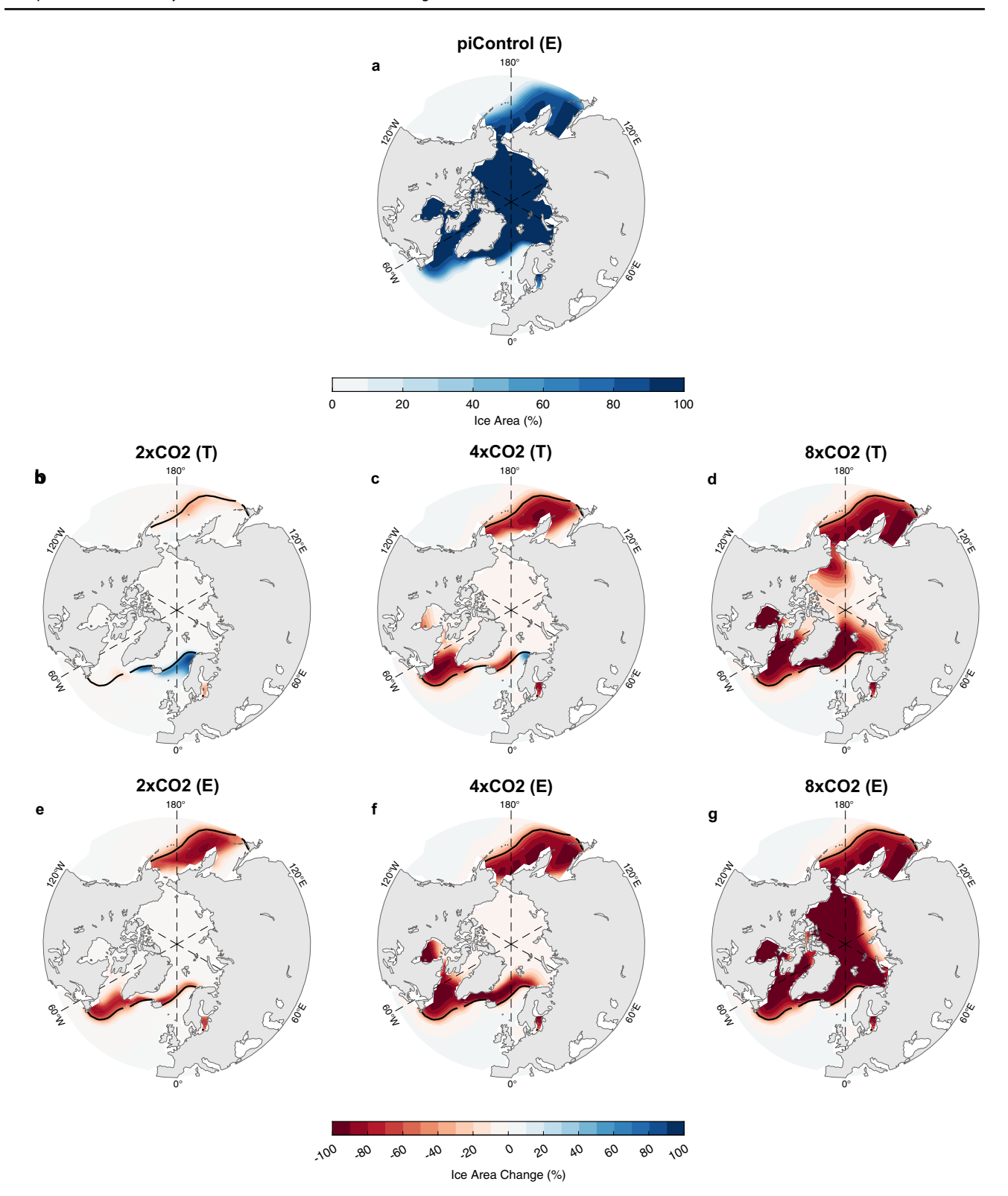


**Fig. 12 a** March sea ice concentration (SIC, ice fraction per grid cell) averaged over the last 1000 years of pre-industrial control data. SIC anomalies relative to pre-industrial control data averaged over (**b-d**) the transient and (**e-g**) equilibrium time periods for the abrupt 2xCO<sub>2</sub>, 4xCO<sub>2</sub>, and 8xCO<sub>2</sub> experiments. In **b-g** blue colors indi-

cate sea ice gain relative to pre-industrial control, and red colors indicate sea ice loss. The black contour indicates the sea ice boundary (defined as SIC of 5%) in the pre-industrial control. The abrupt  $16xCO_2$  experiment loses all sea ice, and is therefore not included in this figure



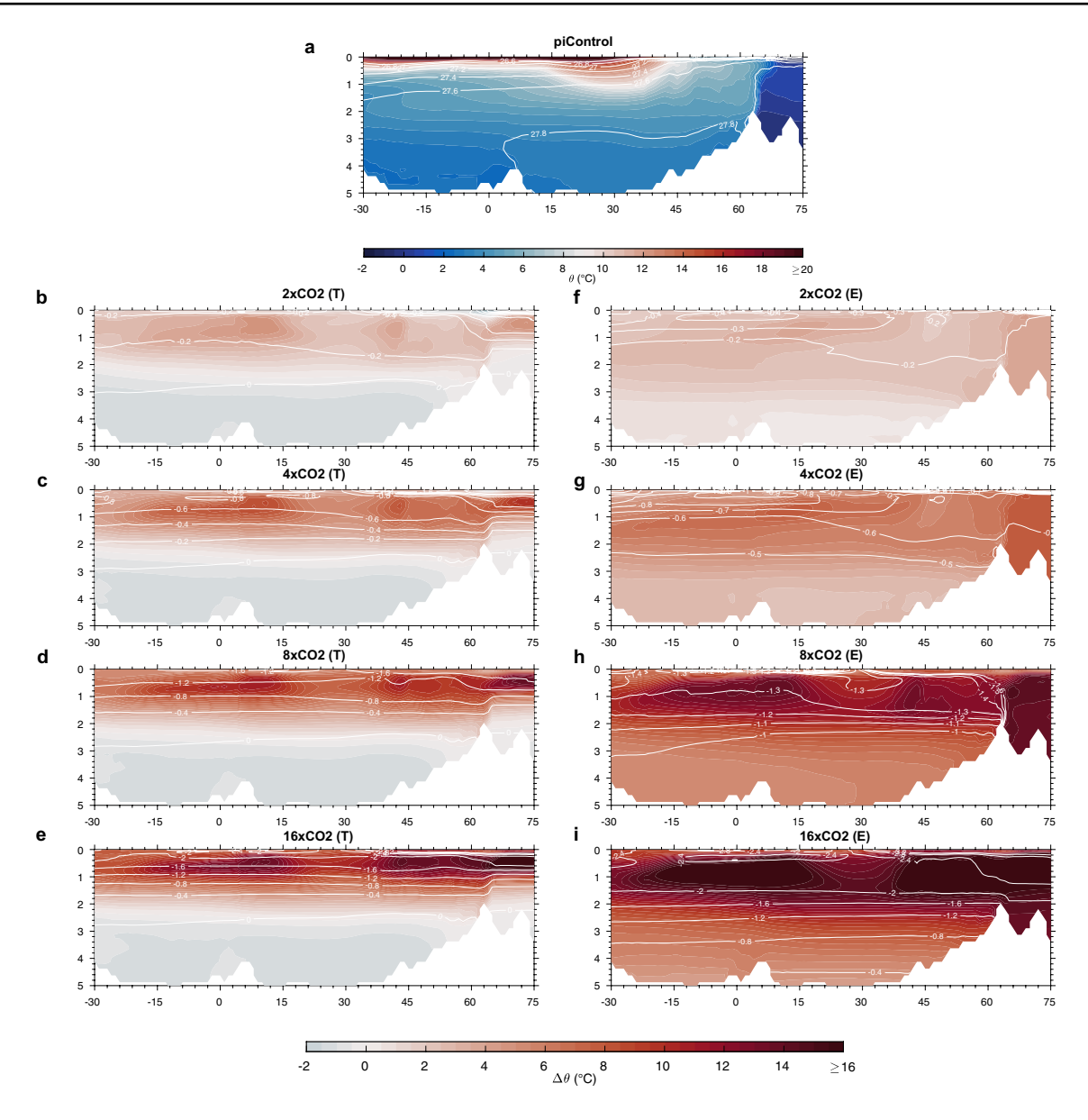


**Fig. 13 a** Zonally averaged North Atlantic temperature in the latitude-depth plane for the last 1000 years of pre-industrial control data. **b-i** Temperature anomalies relative to the Control, for the abrupt 2xCO<sub>2</sub>, 4xCO<sub>2</sub>, 8xCO<sub>2</sub>, and 16xCO<sub>2</sub> experiments, averaged over the transient (**b-e**) and equilibrium time periods **f-i**. White contours indi-

cate potential density anomaly in the top panel and its anomalies relative to the Control in other panels (in kg/m³). Here the North Atlantic basin is taken to be  $60^{\circ}\text{W} \leq \varphi \leq 0^{\circ}\text{W}$  at all latitudes. All data is regridded onto a  $1^{\circ} \times 1^{\circ}$  grid for analysis

the enhanced basin-scale vertical stratification. This warm, relatively saline signal slowly propagates down through the water column but is always strongest close to the surface, as shown by Figs. 13 and 14. This enhanced stratification is maintained when the AMOC recovers and may curtail the depth of the NADW cell. Generally, Fig. 14 suggests that salinity appears to have a muted influence on setting the density structure of the deep ocean.

In the absence of a significant NADW cell, AABW formed in the Southern Ocean encroaches northward through the Atlantic basin at shallower depths. This water mass is present in Fig. 5, and appears as a relatively fresh, but cooler signal below 3 km in Figs. 13 and 14. Importantly, this water mass contributes to setting the density of abyssal waters: potentially reducing the penetration depth of waters sinking in the SPNA and restricting the depth of the NADW cell throughout the North Atlantic basin, as observed in Fig. 5e and f.



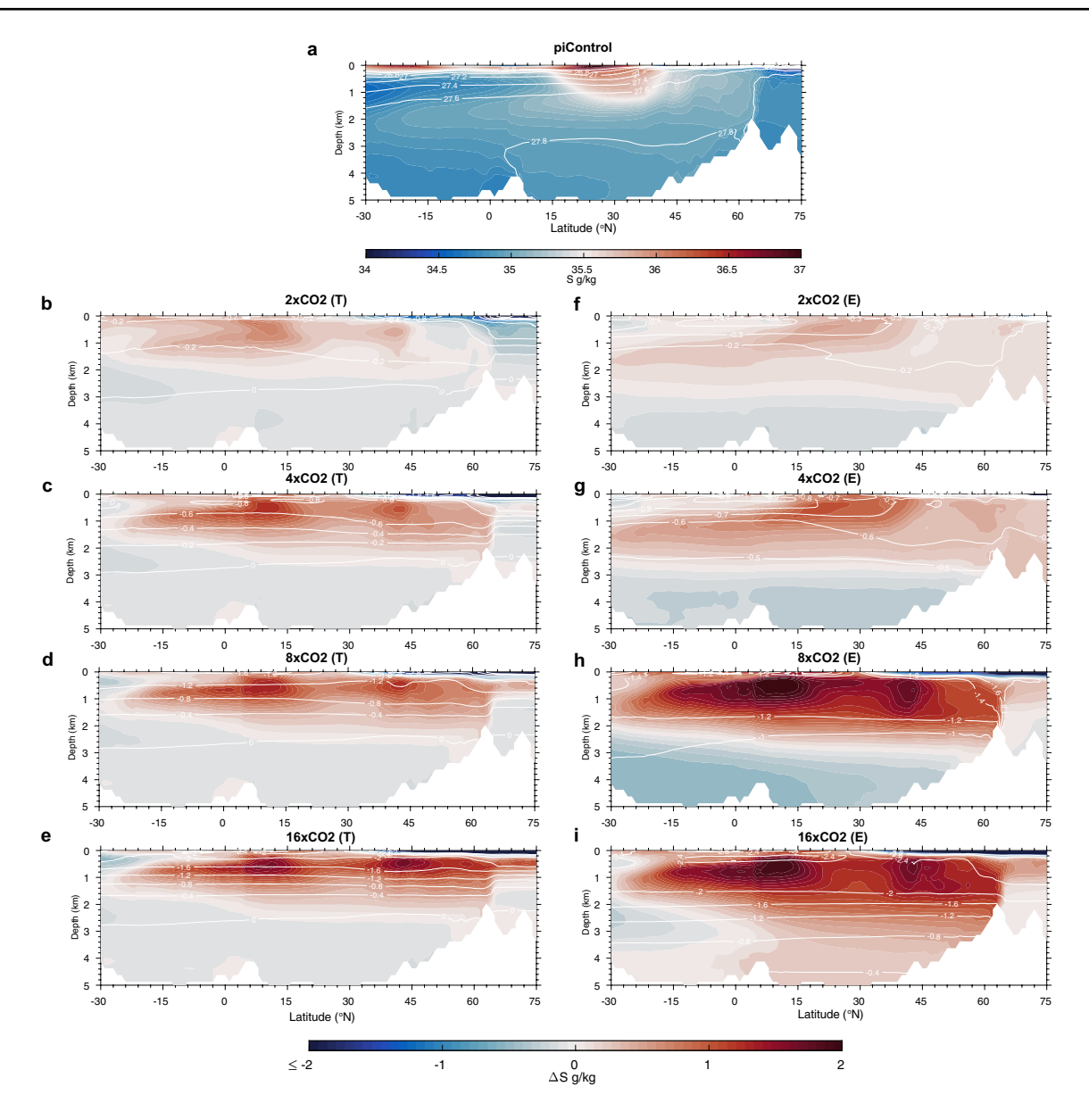


Fig. 14 As in Fig. 13, for salinity

#### 4.3 Mechanisms for AMOC recovery

To discuss potential mechanisms for the AMOC recovery and reinvigoration of NADW deep water formation, we first return to Fig. 3. Figure 3c shows that surface freshening increases vertical ocean stratification in the SPNA in all global warming experiments, although this occurs more slowly in the abrupt  $2xCO_2$  experiment (c.f. Figure 3c). Moreover, in all global warming experiments the thermal contribution to the stratification increases over the first ~ 100 years as upper ocean waters warm more than the deep ocean. Critically, however, as each experiment evolves, the thermal contribution to stratification switches sign: after ~ 100 years for the  $2xCO_2$  and  $4xCO_2$  experiments;

after  $\sim 750$  years for the  $8xCO_2$  experiment; and  $\sim 1500$  years for the  $16xCO_2$  experiment. This is due to an accumulation of heat in the deep ocean, which acts to slowly destabilize the water column in the SPNA. For instance, Fig. 3a shows that after the vertical ocean stratification in the SPNA reaches its maximum (after  $\sim 250$  years in all global warming experiments), the haline contribution continues to slowly increase in magnitude (Fig. 3c).

However, as the AMOC recovery begins to occur in the  $2xCO_2$  and  $4xCO_2$  experiments, the thermal contribution to stratification tends towards a stabilizing effect (i.e., becomes less negative), yet the haline component continues to tend towards a destabilizing effect (i.e., becomes less positive). Therefore, a second process



is clearly required to explain the full recovery. A welldiscussed component of the AMOC recovery in hosing experiments is the salinity advection feedback, which links the increasing surface salinity at higher latitudes to the northward advection of relatively high salinity water from low latitudes by a weakly northward AMOC (Cheng et al. 2018). Figure 4b likely provides supporting evidence for the salinity advection feedback. Here, we observe a slow increase in SSS in the centuries (2xCO<sub>2</sub>) or millennia (4xCO<sub>2</sub>) during the AMOC recovery, coinciding with a reduction in the haline contribution to SPNA stratification (Fig. 3c). This is despite the sustained freshening from the hydrological cycle (Fig. 7a); that is, any increase in surface salinity in the SPNA must originate from ocean advection. There is no indication of a salinity advection feedback in the 8xCO<sub>2</sub> and 16xCO<sub>2</sub> experiments in Fig. 4b, consistent with a water column that is too stable. Therefore, in response to the strong vertical stratification the SPNA water column needs to destabilize sufficiently via deep ocean warming to initiate some deep water formation, at which point the salinity advection feedback can spin-up, generating a recovery to the AMOC which occurs with a timescale of a few centuries.

In this view, our results are consistent with the mechanisms outlined by Bonan et al. 2022 (also in Stouffer and Manabe 2003, however it is less clearly demonstrated in that study), although there is an issue with whether the meridional density gradient actually drives the AMOC (de Boer et al. 2010) or simply reflects AMOC changes. In this study we demonstrate that the interplay between surface freshening and deep ocean warming in the SPNA is dependent upon the strength of the initial radiative forcing, and, therefore upon the magnitude of global warming within a single model. For instance, the amount of deep ocean warming required to destabilize the water column and initiate an AMOC recovery in the 2xCO<sub>2</sub> experiment is less than in the 4xCO<sub>2</sub> experiment. In the 4xCO<sub>2</sub> experiment the transient deep ocean response is characterized by a much more intense (haline and thermal) stratification meaning that deep waters must warm notably to offset this, which takes several millennia as indicated by Fig. 3c and f. It is likely that the magnitude of the increase in high latitude P - E + R and the amount of initial sea ice loss are important in setting the overall timescale for recovery since both factors contribute to increasing the transient high latitude stratification.

In our 8xCO<sub>2</sub> experiment, Fig. 3 indicates that, despite significant deep ocean warming and the associated destabilizing effect in the water column, it is the haline component of stratification that ultimately dominates the bulk stratification as the experiment evolves towards equilibrium (Fig. 3a); Fig. 3 suggests that this would only be amplified in the abrupt 16xCO<sub>2</sub> experiment. This very likely results in a high latitude ocean that remains too stably stratified for

deep convection to occur in these stronger global warming experiments.

# 5 AMOC response to global cooling

Considering Fig. 1a we note that the abrupt  $0.5xCO_2$  experiment exhibits a very different behavior compared to the warming experiments. In Fig. 15 we present transient and end-of-simulation Eulerian-mean streamfunction in the North Atlantic; in Fig. 16 we show the transient and end-of-simulation March MLD, and ice anomalies relative to control; in Fig. 17 we present changes in surface temperature and salinity relative to control.

After reaching a maximum in strength the AMOC in the 0.5xCO<sub>2</sub> experiment slowly decreases, before undergoing a rapid reduction to a much weaker state of overturning after approximately 2000 years of integration. We are hesitant to call this state a collapsed state as the circulation remains at about 7 Sv. Following this sharp reduction, the AMOC undergoes a gradual recovery before abruptly weakening again around the year 3500. The system remains in this state for the remaining 3000 years of integration. This suggests that the quasi-equilibrium state of the system can oscillate between active and inactive (weak) AMOC, potentially indicating millennial variability similar to a Dansgaard-Oeschger (DO) oscillation. This behavior is remarkably different to that observed in Stouffer and Manabe (2003), in which a gradual (although not always monotonic) decrease in overturning strength

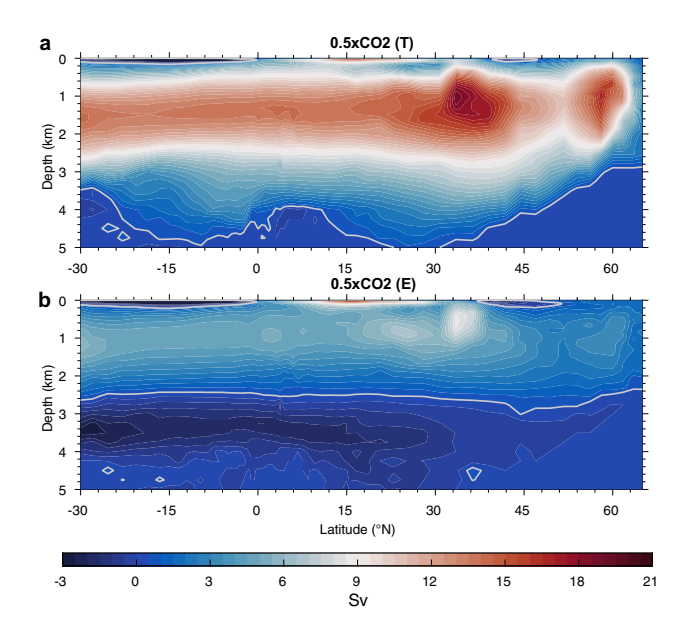


Fig. 15 As in Fig. 8, but for the abrupt  $0.5xCO_2$  experiment: **a** Transient and **b** end of integration (last 1000 years) zonally averaged streamfunction



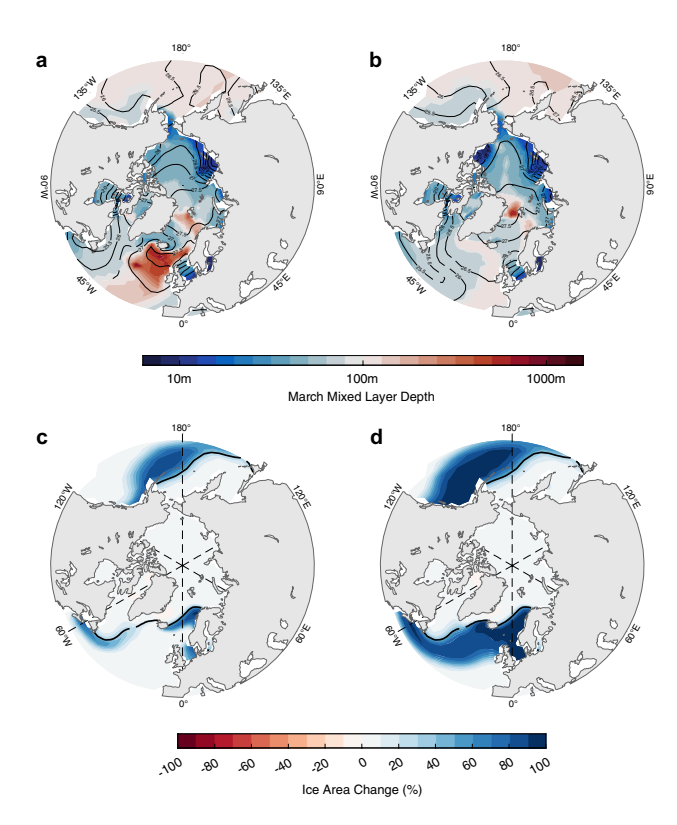


Fig. 16 For the abrupt  $0.5 \text{xCO}_2$  experiment: mixed layer depth averaged over (a) the transient and (b) equilibrium time periods (see the caption for Fig. 9); c, d sea ice concentration (SIC) change for the same time periods, respectively, relative to the pre-industrial control (c.f. Figure 12)

was observed over several millennia, after which the overturning remained low.

On shorter timescales reduced poleward moisture transport increases the surface salinity at high latitudes (Fig. 17). Together with colder surface temperatures (Fig. 17), this decreases ocean vertical stability, accounting for the stronger transient AMOC (also observed in Stouffer and Manabe 2003). However, Fig. 17c shows a freshening northwest of Iceland, which may contribute to the first collapse in AMOC strength through a positive salinity advection feedback, in which these relatively fresh surface waters spread throughout the SPNA and impose an upper-ocean halocline (which is evident in Fig. 17d). Then, in our model the oscillatory behavior describing subsequent AMOC weakening/recoveries could be due to interactions between sea ice and the strength of the AMOC. For instance, we observe large changes in sea ice area which are in antiphase with oscillations in AMOC strength. This is consistent with some simple models of DO events (e.g., Peltier and Vettoretti 2014). In the end of this simulation, the AMOC remains in an inactive (weakened) state, even though there is a possibility that it would recover again. These results will be reported in a follow-up paper focusing on the AMOC behavior in colder climates.

### 6 Discussion and conclusion

In this study we have evaluated the response of the AMOC to a broad range of abrupt radiative forcing scenarios in a fully coupled GCM. We summarize the behavior by plotting AMOC against globally averaged surface air temperature in Fig. 18.

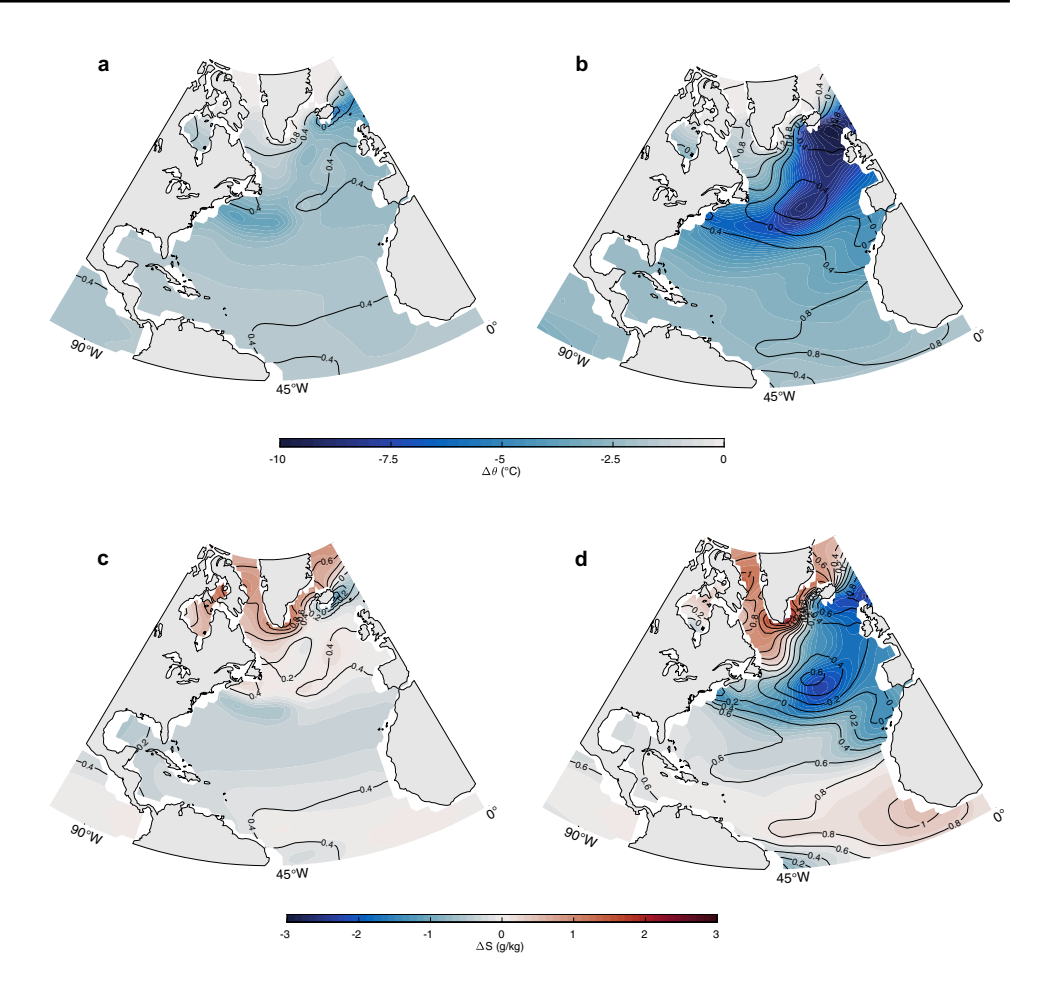
In the 2xCO<sub>2</sub> and 4xCO<sub>2</sub> experiments the AMOC eventually fully recovers its strength after 1,000 and 3500 years, respectively, reaching the same AMOC volume transport as calculated from the piControl experiment. In the 8xCO<sub>2</sub> experiment, even after 10,000 years the full recovery has not happened, even though the AMOC strength slowly increased to ~ 7.5 Sv and stayed constant at this level during the last 5000 years of the simulation. Several lines of evidence indicate that a new equilibrium climate with a weak AMOC may have been reached. However, upper-ocean salinity in the SPNA and deep ocean temperature continued to increase at the end of this simulation, albeit very slowly, which might result in AMOC invigoration at some later time. Although limited to 4250 years, it is likely that the 16xCO<sub>2</sub> experiment would have followed the same scenario, but any solid conclusions about the equilibrium state would require a significantly longer integration time.

Determining the equilibrium response, we have high-lighted and discussed three Northern Hemisphere processes which influence AMOC evolution towards equilibrium. The first is the strengthening and the subsequent decrease in ocean stratification in the SPNA, controlled by an interplay between temperature and salinity. On transient timescales the magnitude of this stratification is determined by the amount of surface freshening. The second factor is a strong Arctic surface temperature amplification which can further enhance SPNA stratification. Finally, the increasing presence of the AABW cell through the North Atlantic basin is likely to influence properties of the deep ocean.

Strong Arctic temperature amplification, which is not simulated in hosing experiments, is able to decrease the SPNA surface density, meaning that more time is required before increasing salinity raises surface densities enough to reinvigorate NADW formation. In turn, melting sea ice also inputs a larger volume of freshwater into the SPNA, thus further reducing the surface density. In fact, enhanced seasonal melting of Arctic sea ice may become a major factor in the freshening of the Arctic and subpolar North Atlantic (Li and Fedorov 2021; Li et al. 2021a, b), although the rate of this input may be important (Kim et al. 2021). Freshening due to Arctic sea ice loss (also discussed by Liu et al. 2019; Li et al. 2021a, b; Li and Fedorov 2021; Bonan et al.



Fig. 17 For the abrupt  $0.5 \text{xCO}_2$  experiment: upper ocean temperature anomalies relative to the pre-industrial control averaged over (a) the transient and (b) equilibrium time periods (c.f. Figure 10); c, d, upper ocean salinity anomalies averaged for the same time periods (c.f. caption for Fig. 11)



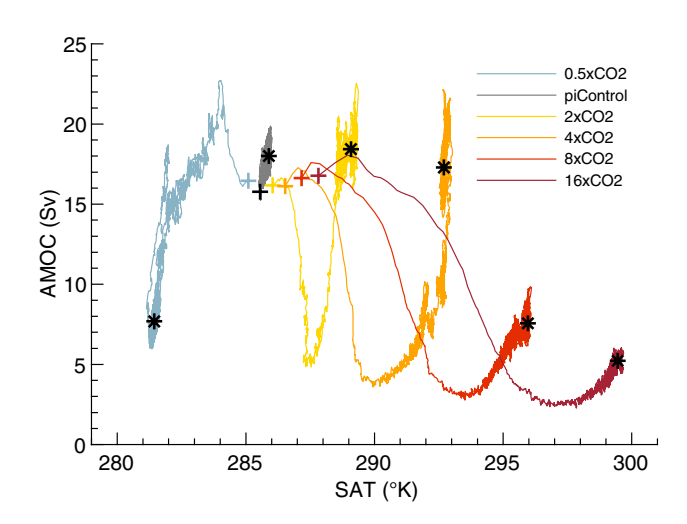


**Fig. 18** Evolution of AMOC strength plotted against globally averaged surface air temperature for all experiments. A 10-year backward mean is applied. Coloured crosses denote the mean over the first year for each experiment; black stars denote the end-of-integration states in each experiment (averaged over the last 1000 years of each experiment). Note that since the first data point in each time series is an average over the first 12 months, the curves for the forced experiments do not start at the piControl

2022), amplified by the salt-advection feedback as part of the AMOC weakening, further delays the AMOC recovery and transition towards equilibrium.

We should stress, however, several limitations of this study. The model we use is relatively coarse (to allow for long integrations). Idealized long higher-resolution and/or adiabatic simulations for the Atlantic basin (no Indo-Pacific) show that the timescales of ocean adjustments/deep ocean ventilation can be much higher (~10,000 years) even in the absence of a strong radiative forcing (Wolfe and Cessi 2011; Haertel and Fedorov 2012; Jansen et al. 2018). Furthermore, with a low-resolution configuration, it is possible that coarse parametrizations of certain processes in the model affect the simulated response.

The second issue is the model's cold bias (Shields et al. 2012), which enhances the areal extent of Northern Hemisphere sea ice, and as such any temperature increase and high latitude freshening (relative to control) in the region is likely to be augmented when compared to other models. The excessive volume of sea ice may also affect the amount of freshening of high latitudes (Li et al. 2021a, b). We further stress that the model analyzed here does not include interactive ice sheets, thus the simulated thermohaline response



may differ from the response in a model that does have this feature, since melting continental ice sheets would further delay AMOC recovery, for example. On the other hand, the model produces a very reasonable AMOC of about 17 Sv with most of the dense water formation occurring in the eastern half of the Subpolar North Atlantic as suggested by recent measurements (Lozier et al. 2019).

Several important implications from this study are worth highlighting. The first one concerns paleoclimates. The model's equilibrium timescales reach the same order of magnitude of the entire Holocene Epoch, and on timescales in which the effect of Milankovitch orbital cycles become significant (Broecker et al. 1985; Barker et al. 2009). In higher resolution simulations those timescales would only increase. This implies that many short paleoclimate simulations, aimed at reproducing particular time slices can still depend on the initial conditions used for those simulations. Likewise, simulation of warm climates may require much longer timescales than typically used. For example, the PlioMIP2 project required integrations of 500 years and longer to simulate the warm Pliocene, which is not enough by an order of magnitude. Brierley and Fedorov (2016) and Burls et al. (2017) used 2500 and 3000 years respectively to simulate warm Pliocene-like climates, but even those integration lengths appear to be somewhat insufficient for simulating a climate equilibrium considering this study.

In paleo studies, a comparison is also made between the modern AMOC and that during the last glacial maximum (LGM). During periods of enhanced glaciation, the ocean is generally thought to be more stratified, in which salinity may be the dominant control on density in the abyssal ocean due to colder ocean temperatures (Adkins et al. 2002). Although atmospheric  $\rm CO_2$  concentrations were markedly lower during the LGM when compared to the present day, an active AMOC persisted (Ganopolski et al. 1998; Bohm et al. 2015). In our  $0.5 \rm x CO_2$  experiment, an active AMOC has not been reached even after ~ 6000 years, which may have implications for LGM simulations that are typically much shorter.

Finally, our results are also important in the context of contemporary global warming. Specifically, if an AMOC collapse does occur at high  $\mathrm{CO}_2$  levels, the recovery will take a long time on the order of ~ 1000 years, unless  $\mathrm{CO}_2$  is rapidly reduced, and this result does not include the melting of the Greenland ice sheet. Thus, if the tipping point determining AMOC collapse is breached, the resulting climatic changes will most likely be irreversible over the coming centuries.

Acknowledgements We thank Kaylea Nelson and the Yale HPC Center for maintaining the high-performance computing environments, and with assistance in setting up the numerical experiments. We thank Natalie Burls who conducted the first portion of the global warming experiments. We also thank three anonymous reviewers whose comments greatly improved the quality of the manuscript.

Author contributions All authors contributed to the study conception and design. Material preparation, data collection and analysis were performed by Paul Edwin Curtis. The first draft of the manuscript was written by Paul Edwin Curtis and all other authors commented on previous versions of the manuscript. All authors read and approved the final manuscript.

**Funding** AVF is supported by NSF (Grant AGS-2053096) and by the ARCHANGE project of the MOGPA program (ANR-18-MPGA-0001, France). PEC is supported by NASA FINESST Fellowship (Grant 80NSSC24K0007).

**Data availability** Data generated during the current study are available from the corresponding author upon reasonable request.

**Code availability** The code files used to generate figures for the current study are available from the corresponding author upon reasonable request.

#### **Declarations**

**Conflict of interest** The authors declare no competing interests.

Ethics approval Not applicable.

Consent for public to participate Not applicable.

#### References

Ackermann L, Danek C, Gierz P et al (2020) AMOC recovery in a multicentennial scenario using a coupled atmosphere-ocean-ice sheet model. Geophys Res Lett 47(16):e2019GL086810. https://doi.org/10.1029/2019GL086810

Adkins JF, McIntyre K, Schrag DP (2002) The salinity, temperature, and  $\delta^{18}$ O of the glacial deep ocean. Science 298:1769–1773. https://doi.org/10.1126/science.1076252

Barker S, Diz P, Vautravers MJ et al (2009) Interhemispheric Atlantic seesaw response during the last deglaciation. Nature 457:1097– 1102. https://doi.org/10.1038/nature07770

Barreiro M, Fedorov A, Pacanowski R et al (2008) Abrupt climate changes: how freshening of the northern Atlantic affects the thermohaline and wind-driven ocean circulations. Annu Rev Earth Planet Sci 36:33–58. https://doi.org/10.1146/annurev.earth.36. 090507.143219

Bellomo K, Angeloni M, Corti S et al (2021) Future climate change shaped by inter-model differences in Atlantic meridional overturning circulation response. Nat Commun 12:3659. https://doi.org/10.1038/s41467-021-24015-w

Boers N (2021) Observation-based early-warning signals for a collapse of the Atlantic meridional overturning circulation. Nat Clim Change 11:680–688. https://doi.org/10.1038/s41558-021-01184-6

Bohm E, Lippold J, Gutjahr M et al (2015) Strong and deep Atlantic meridional overturning circulation during the last glacial cycle. Nature 517:73–76. https://doi.org/10.1038/nature14059

Bonan DB, Thompson AF, Newsom ER et al (2022) Transient and equilibrium responses of the Atlantic overturning circulation to warming in coupled climate models: the role of temperature and salinity. J Clim 35:5173–5193. https://doi.org/10.1175/JCLI-D-21-0912.1

Brierley C, Fedorov AV (2016) Comparing the impacts of Miocene-Pliocene changes in inter-ocean gateways on climate: central



- American seaway, Bering strait, and Indonesia. Earth Planet Sci Lett 444:116–130. https://doi.org/10.1016/j.epsl.2016.03.010
- Broecker WS, Peteet DM, Rind D (1985) Does the ocean-atmosphere system have more than one stable mode of operation? Nature 315:21–26. https://doi.org/10.1038/315021a0
- Buckley MW, Marshall J (2016) Observations, inferences, and mechanisms of the Atlantic meridional overturning circulation: a review. Rev Geophys 54:5–63. https://doi.org/10.1002/2015R G000493
- Burls N, Fedorov AV, Sigman DM et al (2017) Active Pacific meridional overturning circulation (PMOC) during the warm Pliocene. Sci Adv 3(e1700):156. https://doi.org/10.1126/sciadv.1700156
- Caesar L, Rahmstorf S, Robinson S et al (2018) Observed fingerprint of a weakening Atlantic ocean overturning circulation. Nature 556:191–196. https://doi.org/10.1038/s41586-018-0006-5
- Chafink L, Rossby T (2019) Volume, heat, and freshwater divergences in the Subpolar north Atlantic suggest the Nordic Seas as key to the state of the meridional overturning circulation. Geophys Res Lett 46(9):4799–4808. https://doi.org/10.1029/2019GL082110
- Cheng W, Chiang JC, Zhang D (2013) Atlantic meridional overturning circulation (AMOC) in cmip5 models: RCP and historical simulations. J Clim 26:7187–7197. https://doi.org/10.1175/JCLI-D-12-00496.1
- Cheng W, Weijer W, Kim WM et al (2018) Can the salt-advection feedback be detected in internal variability of the Atlantic meridional overturning circulation? J Clim 31:6649–6667. https://doi.org/ 10.1175/JCLI-D-17-0825.1
- Danabasoglu G, Yeager SG, Bailey D et al (2014) North Atlantic simulations in coordinated ocean-ice reference experiments phase ii (core-ii). Part i: mean states. Ocean Model 73:76–107. https://doi.org/10.1016/j.ocemod.2013.10.005
- Dansgaard W, Johnsen SJ, Clausen HB et al (1993) Evidence for general instability of past climate from a 250-kyr ice-core record. Nature 346:218–220. https://doi.org/10.1038/364218a0
- de Boer AM, Sigman DM, Toggweiler JR et al (2007) Effect of global ocean temperature change on deep ocean ventilation. Paleoceanogr Paleoclimatol 22:PA2210. https://doi.org/10.1029/2005PA001242
- de Boer AM, Gnanadesikan A, Edwards NR, Watson AJ (2010) Meridional density gradients do not control the Atlantic overturning circulation. J Phys Oceanogr 40:368–380. https://doi.org/10.1175/2009JPO4200.1
- Etminan M, Mhyre G, Highwood EJ et al (2016) Radiative forcing of carbon dioxide, methane, and nitrous oxide: a significant revision of the methane radiative forcing. Geophys Res Lett 43:12614–12623. https://doi.org/10.1002/2016GL071930
- Fedorov A, Barreiro M, Boccaletti G et al (2007) The freshening of surface waters in high latitudes: effects on the thermohaline and wind-driven circulations. J Phys Oceanogr 37:896–907. https://doi.org/10.1175/JPO3033.1
- Fedorov AV, Burls NJ, Lawrence KT et al (2015) Tightly linked zonal and meridional sea surface temperature gradients over the past five million years. Nature Geosci 8(12):975–980. https://doi.org/10.1038/ngeo2577
- Ferrari R, Jansen MF, Adkins JF et al (2014) Antarctic sea ice control on ocean circulation in present and glacial climates. Proc Natl Acad Sci USA 111:8753–8758. https://doi.org/10.1073/pnas. 1323922111
- Frajka-Williams E, Ansorge IJ, Baehr J et al (2019) Atlantic meridional overturning circulation: observed transports and variability. Front Mar Sci. https://doi.org/10.3389/fmars.2019.00260
- Ganopolski A, Rahmstorf S, Petoukhov V et al (1998) Simulation of modern and glacial climates with a coupled global model of intermediate complexity. Nature 391:351–356. https://doi.org/ 10.1038/34839

- Gent PR (2018) A commentary on the Atlantic Meridional Overturning Circulation stability in climate models. Ocean Model 122:57–66. https://doi.org/10.1016/j.ocemod.2017.12.006
- Gent PR, Danabasoglu G, Donner LJ et al (2011) The community climate system model version 4. J Clim 24:4974–4991. https://doi.org/10.1175/2011JCLI4083.1
- Gnanadesikan A (1999) A simple predictive model for the structure of the oceanic pycnocline. Science 283:2077–2079. https://doi.org/10.1126/science.283.5410.2077
- Gregory JM, Dixon KW, Stouffer RJ et al (2005) A model intercomparison of changes in the Atlantic thermohaline circulation in response to increasing atmospheric CO<sub>2</sub> concentration. Geophys Res Lett. https://doi.org/10.1029/2005GL023209
- Haertel P, Fedorov AV (2012) The ventilated ocean. J Phys Oceanogr 42:141–164. https://doi.org/10.1175/2011JPO4590.1
- Haskins RK, Oliver KIC, Jackson LC et al (2019) Explaining asymmetry between weakening and recovery of the AMOC in a coupled climate model. Clim Dyn 53:67–79. https://doi.org/10.1007/s00382-018-4570-z
- Held IM, Soden BJ (2006) Robust responses of the hydrological cycle to global warming. J Clim 19:5686–5699. https://doi.org/10.1175/JCLI3990.1
- Hofmann M, Rahmstorf S (2009) On the stability of the Atlantic meridional overturning circulation. Proc Natl Acad Sci USA 49:20584–20589. https://doi.org/10.1073/pnas.0909146106
- Huezé C (2017) North Atlantic deep water formation and AMOC in cmip5 models. Ocean Sci 13:609–622. https://doi.org/10. 5194/os-13-609-2017
- Huezé C (2021) Antarctic bottom water and north Atlantic deep water in cmip6 models. Ocean Sci 17:59–90. https://doi.org/ 10.5194/os-17-59-2021
- Jackson LC (2013) Shutdown and recovery of the AMOC in a coupled global climate model: the role of the advective feedback. Geophys Res Lett 40(6):1182–1188. https://doi.org/10.1002/grl.50289
- Jackson LC, Kahana R, Graham T et al (2015) Global and European climate impacts of a slowdown of the AMOC in a high resolution GCM. Clim Dyn 45:3299–3316. https://doi.org/10.1007/ s00382-015-2540-2
- Jackson LC, Biastoch A, Buckley MW et al (2022) The evolution of the north Atlantic meridional overturning circulation since 1980. Nat Rev Earth Environ 3:241–254. https://doi.org/10. 1038/s43017-022-00263-2
- Jackson LC, Alastrué de Asenio E, Bellomo K et al (2023) Understanding AMOC stability: the North Atlantic hosing model intercomparison project. Geosci Model Dev 16:1975–1995. https://doi.org/10.5194/gmd-16-1975-2023
- Jansen MF, Nadeau LP, Merlis TM (2018) Transient versus equilibrium response of the ocean's overturning circulation to warming. J Clim 31:5147–5163. https://doi.org/10.1175/JCLI-D-17-0797.1
- Kiel P, Mauritsen T, Jungclaus J et al (2020) Multiple drivers of the north Atlantic warming hole. Nat Clim Change 10:667–671. https://doi.org/10.1038/s41558-020-0819-8
- Killworth PD (1983) Deep convection in the world ocean. Rev Geophys and Space Phys 21:1–26. https://doi.org/10.1029/RG021i001p00001
- Kim HJ, An SI, Kim SK et al (2021) Feedback processes modulating the sensitivity of Atlantic thermohaline circulation to freshwater forcing timescales. J Clim 34:5081–5092. https://doi.org/ 10.1175/JCLI-D-20-0897.1
- Klockmann M, Mikolajewicz U, Marotzke J (2018) Two AMOC states in response to decreasing greenhouse gas concentrations in the coupled climate model MPI-ESM. J Clim 31:7969–7984. https://doi.org/10.1175/JCLI-D-17-0859.1



- Lenton TM, Held H, Kriegler E et al (2008) Tipping elements in the earth's climate system. Proc Natl Acad Sci USA 105:1786–1793. https://doi.org/10.1073/pnas.0705414105
- Li H, Fedorov AV (2021) Persistent freshening of the arctic ocean and changes in the north Atlantic salinity caused by arctic sea ice decline. Clim Dyn 57:2995–3013. https://doi.org/10.1007/ s00382-021-05850-5
- Li H, Fedorov A, Liu W (2021a) AMOC stability and diverging response to arctic sea ice decline in two climate models. J Clim 34:5443–5460. https://doi.org/10.1175/JCLI-D-20-0572.1
- Li F, Lozier MS, Bacon S et al (2021b) Subpolar north Atlantic western boundary density anomalies and the Meridional overturning circulation. Nat Commun 12:3002. https://doi.org/10.1038/s41467-021-23350-2
- Liu W, Xie S-P, Liu Z, Zhu J (2017) Overlooked possibility of a collapsed Atlantic meridional overturning circulation in warming climates. Sci Adv 3:e1601666. https://doi.org/10.1126/sciadv. 1601666
- Liu W, Fedorov A, Sévellec F (2019) The mechanisms of the Atlantic meridional overturning circulation slowdown induced by arctic sea ice decline. J Clim 32:977–996. https://doi.org/10.1175/ JCLI-D-18-0231.1
- Liu W, Fedorov AV, Xie SP et al (2020) Climate impacts of a weakened Atlantic meridional overturning circulation in a warming climate. Sci Adv 6:eaaz4876. https://doi.org/10.1126/sciadv.aaz4876
- Lozier MS, Li F, Bacon S (2019) A sea change in our view of overturning in the subpolar North Atlantic. Science 363(6426):516–521. https://doi.org/10.1126/science.aau6592
- Manabe S, Stouffer RJ (1988) Two stable equilibria of the coupled ocean-atmosphere model. J Clim 1:841–866. https://doi.org/10. 1175/1520-0442(1988)001%3C0841:TSEOAC%3E2.0.CO;2
- Manabe S, Stouffer RJ (1993) Century-scale effects of increased atmospheric CO<sub>2</sub> on the ocean-atmosphere system. Nature 364:215–218. https://doi.org/10.1038/364215a0
- Manabe S, Stouffer RJ (1995) Simulation of abrupt climate change induced by freshwater input to the North Atlantic Ocean. Nature 378:165–167. https://doi.org/10.1038/378165a0
- Marshall J, Schott F (1999) Open-ocean convection: observations, theory, and models. Rev Geophys 37(1):1–64. https://doi.org/10.1029/98RG02739
- Marshall J, Speer K (2012) Closure of the meridional overturning circulation through southern ocean upwelling. Nat Geosci 5:171–180. https://doi.org/10.1038/ngeo1391
- Marzocchi A, Jansen MF (2017) Connecting Antarctic sea ice to deep-ocean circulation in modern and glacial climate simulations. Geophys Res Lett 44:6286–6295. https://doi.org/10.1002/ 2017GL073936
- McCreary JP, Lu P (1994) Interaction between the subtropical and equatorial ocean circulations: the subtropical cell. J Phys Oceanogr 24:466–497. https://doi.org/10.1038/s41586-018-0006-5
- McKay DIA, Staal A, Abrams JF et al (2022) Exceeding 1.5°C global warming could trigger multiple climate tipping points. Science 377(6611):eabn7950. https://doi.org/10.1126/science.abn7950
- Mecking JV, Drijfhout SS, Jackson LC, Graham T (2016) Stable AMOC off state in an eddy-permitting coupled climate model. Clim Dyn 47:2455–2470. https://doi.org/10.1007/s00382-016-2975-0
- Mikolajewicz U, Voss R (2000) The role of the individual air-sea flux components in CO<sub>2</sub>-induced changes of the ocean's circulation and climate. Clim Dyn 16:627–642. https://doi.org/10.1007/s003820000066
- Moat BI, Smeed DA, Frajka-Williams E et al (2020) Pending recovery in the strength of the meridional overturning circulation at 26°N.

  Ocean Sci 16:863–874. https://doi.org/10.5194/os-16-863-2020
- Moreno-Chamarro E, Marshall J, Delworth TL (2020) Linking ITCZ migrations to the AMOC and north Atlantic/Pacific SST

- decadal variability. J Clim 33:893–905. https://doi.org/10.1175/ JCLI-D-19-0258.1
- Nikurashin M, Vallis GK (2012) A theory of the interhemispheric meridional overturning circulation and associated stratification. J Phys Oceanogr 42:1652–1667. https://doi.org/10.1175/JPO-D-11-0189.1
- Peltier WR, Vettoretti G (2014) Dansgaard-Oeschger oscillations predicted in a comprehensive model of glacial climate: a "kicked" salt oscillator in the Atlantic. Geophys Res Lett 41(20):7306–7313. https://doi.org/10.1002/2014GL061413
- Rahmstorf S (1995) Bifurcations of the Atlantic thermohaline circulation in response to changes in the hydrological cycle. Nature 378:145–149. https://doi.org/10.1038/378145a0
- Rahmstorf S (2002) Ocean circulation and climate during the past 120,000 years. Nature 419:207–214. https://doi.org/10.1038/nature01090
- Rohling EJ, Sluijs A, Dijkstra HA et al (2012) Making sense of palaeoclimate sensitivity. Nature 491:683–691. https://doi.org/10.1038/nature11574
- Rooth C (1982) Hydrology and ocean circulation. Progr Oceanogr 11:131–149. https://doi.org/10.1016/0079-6611(82)90006-4
- Rugenstein M, Bloch-Johnson J, Abe-Ouchi A et al (2019) LongRun-MIP: motivation and design for a large collection of millenniallength AOGCM simulations. Bull Am Meteorol Soc 100:2551– 2570. https://doi.org/10.1175/BAMS-D-19-0068.1
- Sévellec F, Fedorov AV (2011) Stability of the Atlantic meridional overturning circulation and stratification in a zonally averaged ocean model: effects of freshwater flux, southern ocean winds, and diapycnal diffusion. Deep-Sea Res II: Top Stud Oceanogr 58:1927–1943. https://doi.org/10.1016/j.dsr2.2010.10.070
- Sévellec F, Fedorov A, Liu W (2017) Arctic sea-ice decline weakens the Atlantic meridional overturning circulation. Nat Clim Change 7:604–610. https://doi.org/10.1038/nclimate3353
- Shields CA, Bailey DA, Danabasoglu G et al (2012) The low-resolution CCSM4. J Clim 25:3993–4014. https://doi.org/10.1175/ JCLI-D-11-00260.1
- Shin SI, Liu ZG, Otto-Bliesner BL et al (2003) Southern ocean sea-ice control of the glacial north Atlantic thermohaline circulation. Geophs Res Lett 30:1096. https://doi.org/10.1029/2002GL0155 13
- Sigmond M, Fyfe JC, Saenko OA et al (2020) Ongoing AMOC and related sea-level and temperature changes after achieving the Paris targets. Nat Clim Chang 10:672–677. https://doi.org/10.1038/s41558-020-0786-0
- Speer K, Tziperman E (1992) Rates of water mass formation in the north Atlantic Ocean. J Phys Oceanogr 22:93–104. https://doi.org/10.1175/1520-0485(1992)022%3C0093:ROWMFI%3E2.0. CO:2
- Stommel H (1961) Thermohaline convection with two stable regimes of flow. Tellus 13:224–230. https://doi.org/10.1111/j.2153-3490. 1961.tb00079.x
- Stouffer RJ (2004) Time scales of climate response. J Clim 17:209–217. https://doi.org/10.1175/1520-0442(2004)017%3C0209: TSOCR%3E2.0.CO;2
- Stouffer RJ, Manabe S (2003) Equilibrium response of thermohaline circulation to large changes in atmospheric CO<sub>2</sub> concentration. Clim Dyn 20:759–773. https://doi.org/10.1007/s00382-002-0302-4
- Stouffer RJ, Yin J, Gregory JM et al (2006) Investigating the causes of the response of the thermohaline circulation to past and future climate changes. J Clim 19:1365–1387. https://doi.org/10.1175/JCL13689.1
- Thomas MD, Fedorov AV (2019) Mechanisms and impacts of a partial AMOC recovery under enhanced freshwater forcing. Geophys Res Lett 46(6):3308–3316. https://doi.org/10.1029/2018GL080442



- Timmermann A, Okumura Y, An SI et al (2007) The influence of a weakening of the Atlantic meridional overturning circulation on ENSO. J Clim 20:4899–4919. https://doi.org/10.1175/JCLI4 283.1
- Toggweiler JR, Samuels B (1998) On the ocean's large-scale circulation near the limit of no vertical mixing. J Phys Oceanogr 28:1832–1852. https://doi.org/10.1175/1520-0485(1998)028% 3C1832:OTOSLS%3E2.0.CO;2
- Trenberth KE, Zhang Y, Fasullo JT et al (2019) Observation-based estimate of global and basin ocean meridional heat transport time series. J Clim 32:4567–4583. https://doi.org/10.1175/JCLI-D-18-0872.1
- Vellinga M, Wood RA (2002) Global climatic impacts of a collapse of the Atlantic thermohaline circulation. Clim Change 54:251–267. https://doi.org/10.1023/A:1016168827653
- Warren BA (1983) Why is no deep water formed in the north Pacific? J Mar Res 41:327–347. https://doi.org/10.1357/002224083788520 207
- Weaver AJ, Sedlacek J, Eby M et al (2012) Stability of the Atlantic meridional overturning circulation: a model intercomparison. Geophys Res Lett. https://doi.org/10.1029/2012GL053763
- Weijer W, Cheng W, Drijfhout SS et al (2019) Stability of the Atlantic meridional overturning circulation: a review and synthesis. J Geophys Res Oceans 124:5336–5375. https://doi.org/10.1029/2019JC015083
- Weijer W, Cheng W, Garuba OA et al (2020) Cmip6 models predict significant 21st century decline of the Atlantic meridional overturning circulation. Geophys Res Lett 47(12):e2019GL086075. https://doi.org/10.1029/2019GL086075
- Wiebe EC, Weaver AJ (1999) On the sensitivity of global warming experiments to the parametrisation of sub-grid scale ocean mixing. Clim Dyn 15:875–893. https://doi.org/10.1007/s003820050319
- Wolfe CL, Cessi P (2011) The adiabatic pole-to-pole overturning circulation. J Phys Oceanogr 41:1795–1810. https://doi.org/10.1175/2011JPO4570.1
- Wolfe CL, Cessi P (2014) Salt feedback in the adiabatic overturning circulation. J Phys Oceanogr 44:1175–1194. https://doi.org/10.1175/jpo-d-13-0154.1

- Yan X, Zhang R, Knutson TR (2017) The role of Atlantic overturning circulation in the recent decline of Atlantic major hurricane frequency. Nat Commun. https://doi.org/10.1038/s41467-017-01377-8
- Yin J, Stouffer RJ (2007) Comparison of the stability of the Atlantic thermohaline circulation in two coupled atmosphere-ocean general circulation models. J Clim 20:4293–4315. https://doi.org/ 10.1175/JCLI4256.1
- Zhang R, Delworth TL (2005) Simulated tropical response to a substantial weakening of the Atlantic thermohaline circulation. J Clim 18(12):1853–1860. https://doi.org/10.1175/JCL13460.1
- Zhang R, Delworth TL (2006) Impact of Atlantic multidecadal oscillations on India/Sahel rainfall and Atlantic hurricanes. Geophys Res Lett. https://doi.org/10.1029/2006GL026267
- Zhang R, Thomas M (2021) Horizontal circulation across density surfaces contributes substantially to the long-term mean northern Atlantic meridional overturning circulation. Commun Earth Environ 2:112. https://doi.org/10.1038/s43247-021-00182-y
- Zhang X, Knorr G, Lohmann G et al (2017) Abrupt north Atlantic circulation changes in response to gradual CO<sub>2</sub> forcing in a glacial climate state. Nat Geosci 10:518–523. https://doi.org/10.1038/ngeo2974
- Zhu J, Liu Z, Zhang J et al (2015) AMOC response to global warming: dependence on the background climate and response timescale. Clim Dyn 44:3449–3468. https://doi.org/10.1007/s00382-014-2165-x

**Publisher's Note** Springer Nature remains neutral with regard to jurisdictional claims in published maps and institutional affiliations.

Springer Nature or its licensor (e.g. a society or other partner) holds exclusive rights to this article under a publishing agreement with the author(s) or other rightsholder(s); author self-archiving of the accepted manuscript version of this article is solely governed by the terms of such publishing agreement and applicable law.

